AD-A168 951 ANALYSIS OF THE NONLINEAR STABILITY OF CIRCULAR COUETTE FLOW(U) VIRGINIA POLYTECHNIC INST AND STATE UNIV BLACKSBURG DEPT OF E.. T HERBERT JUN 86 1/1

UNCLASSIFIED ARO-18744.15-MA DAAG29-82-K-0129 F/G 20/4 NL

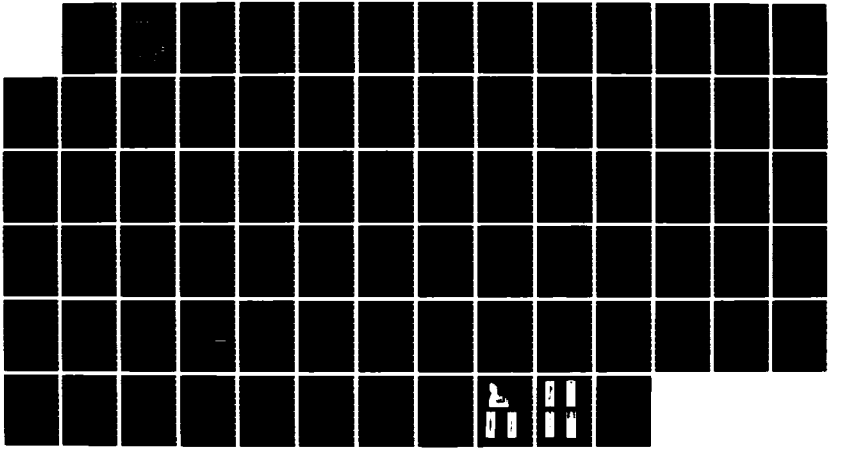

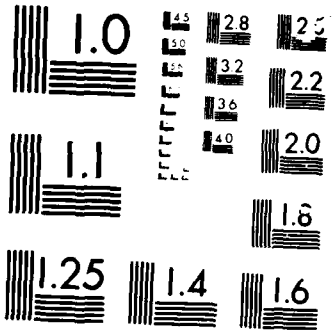
1.0
1.1
1.25
1.4
1.6
1.8
2.0
2.2
2.8
3.2
3.6
4.0

(2)

COLLEGE OF ENGINEERING

FINAL REPORT

Army Research Office
Contract DAAG29-82-K-0129

Analysis of the Nonlinear Stability of Circular Couette Flow

by

Thorwald Herbert

Department of Engineering Science and Mechanics
Virginia Polytechnic Institute and State University
Blacksburg, Virginia 24061

VIRGINIA POLYTECHNIC INSTITUTE AND STATE UNIVERSITY

BLACKSBURG, VIRGINIA

FINAL REPORT

Army Research Office
Contract DAAG29-82-K-0129

Analysis of the Nonlinear Stability of Circular Couette Flow

by

Thorwald Herbert

Department of Engineering Science and Mechanics
Virginia Polytechnic Institute and State University
Blacksburg, Virginia 24061

June 1986

UNCLASSIFIED

SECURITY CLASSIFICATION OF THIS PAGE (When Data Entered)

REPORT DOCUMENTATION PAGE		READ INSTRUCTIONS BEFORE COMPLETING FORM
1. REPORT NUMBER ARO 18744.15-MA	2. GOVT ACCESSION NO. N/A	3. RECIPIENT'S CATALOG NUMBER N/A
4. TITLE (and Subtitle) ANALYSIS OF THE NONLINEAR STABILITY OF CIRCULAR COUETTE FLOW		5. TYPE OF REPORT & PERIOD COVERED Final Report 06/16/1982 - 12/15/1985 6. PERFORMING ORG. REPORT NUMBER
7. AUTHOR(s) Thorwald Herbert		8. CONTRACT OR GRANT NUMBER(s) DAAG 29-82-K-0129
9. PERFORMING ORGANIZATION NAME AND ADDRESS Virginia Polytechnic Institute and State Univ. ESM Dept., Blacksburg, VA 24061		10. PROGRAM ELEMENT, PROJECT, TASK AREA & WORK UNIT NUMBERS
11. CONTROLLING OFFICE NAME AND ADDRESS U. S. Army Research Office Post Office Box 12211 Research Triangle Park, NC 27709		12. REPORT DATE June 1986 13. NUMBER OF PAGES
14. MONITORING AGENCY NAME & ADDRESS (if different from Controlling Office)		15. SECURITY CLASS. (of this report) Unclassified 15a. DECLASSIFICATION/DOWNGRADING SCHEDULE

16. DISTRIBUTION STATEMENT (of this Report)

Approved for public release; distribution unlimited.

17. DISTRIBUTION STATEMENT (of the abstract entered in Block 20, if different from Report)

NA

18. SUPPLEMENTARY NOTES

The view, opinions, and/or findings contained in this report are those of the author(s) and should not be construed as an official Department of the Army position, policy, or decision, unless so designated by other documentation.

19. KEY WORDS (Continue on reverse side if necessary and identify by block number)

flight instability of liquid-filled shells
stability of Taylor-vortex flow
perturbation methods, spectral methods
flow visualization

20. ABSTRACT (Continue on reverse side if necessary and identify by block number)

DD FORM 1 JAN 73 1473 EDITION OF 1 NOV 65 IS OBSOLETE

UNCLASSIFIED

SECURITY CLASSIFICATION OF THIS PAGE (When Data Entered)

ABSTRACT

The work under this contract aimed at three major goals:

(1) *Reveal the origin of the despin moment that may cause severe flight instability of spin-stabilized artillery shells with liquid payloads.* After evaluation of the experimental data and analysis of the equations for the fluid motion in a spinning and nutating cylinder, we have developed a simple model of this flow. For a finite segment of an infinite cylinder, this model provides the flow field and the viscous contribution to the liquid moments in analytical form. At low Reynolds number, the flow field agrees well with computational results for the center section of a cylinder of aspect ratio 4.3. The roll moment associated with this flow agrees with experimental data for a wide range of Reynolds numbers. Guided by the analytical work, a spectral code is currently being developed for solving linearized and fully nonlinear equations of motion in a finite length cylinder. A small test fixture has been built and used for visualization of the flow pattern under various conditions.

(2) *Explore the potential of high-order perturbation methods for describing nonlinear properties of single modes and mode interactions in hydrodynamic stability.* We have chosen plane Poiseuille flow and circular Couette flow as prototype flows. Use of state-of-the-art techniques for analyzing and improving the convergence of perturbation series has in many cases shown tremendous potential for describing the nonlinear properties of single modes at large amplitudes. However, numerous pitfalls of this method have been encountered that range from zero radius of convergence to the inability of obtaining the solution near and beyond branch cuts. For multiple modes, the computational effort increases dramatically and may not pay off due to lacking intuition in selecting relevant and complete models of mode interaction.

(3) *Analyze the mechanism of state selection in unstable circular Couette flow.* While linear stability theory predicts instability of circular Couette flow with respect to Taylor vortices in a wide band of axial wavenumbers, experiments find stable vortices only in a small neighborhood of the critical wavenumber. We have applied various methods in order to understand this problem of wavenumber selection. Most successful was a numerical study on the evolution of Taylor vortices from a discrete spectrum of initial disturbances. We found that for sufficiently large Taylor numbers, the linear instability with respect to vortices of small wavenumber does not lead to a finite-amplitude equilibrium state associated with this wavenumber. Disturbances of small wavenumber, although stable according to the linear theory, may lead to Taylor vortices of larger wavenumber. Both, wavenumbers and initial amplitudes, of the disturbances play a role in the selection process. We found jump phenomena, amplitude overshoot and oscillatory solutions, and finally, a relation between the band-width of stable vortices and the finite length of the cylinders used in experiments. Many of the numerical results are supported by results of multi-mode perturbation techniques.

TABLE OF CONTENTS

1. Accomplishments

The working period for this contract was originally 82/06/16 - 85/06/15, but has been extended until 85/12/15 in order to provide for completing the Ph.D. theses conducted under this contract. During this working period, the following personnel has been partly supported under contract DAAG29-82-K-0129:

Thorwald Herbert, Professor, Principal Investigator
William S. Saric, Professor, Principal Investigator
Saad Ragab, Assistant Professor
Charles Thompson, Assistant Professor
Joseph W. Croswell, Graduate Student (M.S. level)
Relja Zivojnovic , Graduate Student (M.S. level)
K. Sethuramalingam, Graduate Student (Ph.D. level)
Ri-Hua Li, Graduate Student (Ph.D. level)
Charlotte R. Hawley, Research Specialist
Fabio Bertolotti, Deb-Asish Ghosh (hourly wage students)

David Pierpont, undergraduate student, has been involved in the experimental work on visualization of the flow in a spinning and nutating cylinder at no cost (Senior Project). The study of the internal flow in a fluid-filled cylinder in spinning and nutating motion has been jointly supported by this Contract and by the U.S. Army AMCCOM, Contract DAAK11-83-K-0011. The work of Ri-Hua Li and K. Sethuramalingam has been jointly supported by the Army Research Office and by the National Science Foundation under Contract MEA-8120935.

1.1 Presentations

Research findings have been reported at the following conferences:

(1) Th. Herbert and W. S. Saric, "Stability Analysis of the Motion of Confined Rotating Fluids," 28th Conference of Army Mathematicians, Bethesda, Maryland (June 1982).

(2) Th. Herbert and W. S. Saric, "Modelling of the Viscous Fluid Motion in a Precessing Non-Rigid Payload," Aeroballistics and Fluid Dynamics 1982 Research and Technology Conference, Downington, Pennsylvania

(1982).

(3) Th. Herbert, "The Flow of Highly Viscous Fluid in a Spinning and Nutating Cylinder," 1983 Scientific Conference on Chemical Defense Research, Aberdeen Proving Ground, Maryland (Nov. 1983)

(4) Th. Herbert, "Nonlinear Effects in Hydrodynamic Stability," AGARD Special Course on Stability and Transition of Laminar Flow, von Kármán Institute, Rhode-Saint-Genèse, Belgium (Mar. 1984).

(5) Th. Herbert, "Highly Viscous Fluid Flow in a Spinning and Nutating Cylinder," Second Army Conference on Applied Mathematics and Computing, Troy, New York (May 1984).

(6) Th. Herbert, "Instability of the Viscous Flow in a Spinning and Nutating Cylinder," ARO Workshop on Liquid-Filled Shells, Aberdeen Proving Ground, Maryland (Sept. 1984).

(7) Th. Herbert, "Instability of the Viscous Flow in a Spinning and Nutating Cylinder," Scientific Conference on Chemical Defense Research, Aberdeen Proving Ground, Maryland (Nov. 1984).

(8) Th. Herbert and R. H. Li, "State Selection for Taylor-Vortex Flow," Third Army Conference on Applied Mathematics and Computing, Atlanta, Georgia (May 1985)

(9) Th. Herbert and R. H. Li, "On the Domain of Stable Taylor-Vortex Flow," Proc. Conference on Mathematics Applied to Fluid Mechanics and Stability - Dedicated in Memory of Richard C. DiPrima, Troy, New York (Sept. 1985).

(10) Th. Herbert, "Zur Stabilität axialsymmetrischer Taylor Wirbel," Institut für Aerodynamik und Gasdynamik, Universität Stuttgart (Oct. 1985).

(11) Th. Herbert, "On the Fluid Motion in Liquid-Filled Shells," Scientific Conference on Chemical Defense Research, Aberdeen Proving Ground, Maryland (Nov. 1985).

(12) Th. Herbert and R. H. Li, "State Selection in Taylor-Vortex Flow," Meeting of the Division of Fluid Mechanics of the American Physical

Society, Tucson, Arizona (Nov. 1985).

(13) An abstract of a paper entitled "Fluid Motion in Liquid-Filled Shells" by Th. Herbert has been submitted for presentation at the Army Conf. on Mathematics and Computing, Ithaca, New York (May 1986)

1.2. Theses and Degrees Awarded

(1) Ri-Hua Li, "Analysis for Taylor Vortex Flow," Ph.D. Thesis, Virginia Polytechnic Institute and State University, Blacksburg, Virginia (1986). Ph. D. awarded March 1986

(2) K. Sethuramalingam, "High-Order Parameter Expansions for Equilibrium States in Plane Poiseuille Flow," Ph.D. Thesis, Virginia Polytechnic Institute and State University, Blacksburg, Virginia. In preparation.

(3) David Pierpont, "Design of an Experiment for Visualization of the Flow in a Spinning and Nutating Cylinder," Senior Project Report, Virginia Polytechnic Institute and State University, Blacksburg, Virginia (1985).

1.3. Publications

A selection of results has been published in the following papers:

(1) Th. Herbert "Fluid Motion in a Rotating and Nutating Container," Report partly prepared under Scientific Services Program (1982), Published as Report CRDC-CR-84087 (1984).

(2) Th. Herbert "The Flow of Highly Viscous Fluid in a Spinning and Nutating Cylinder," 1983 Scientific Conference on Chemical Defense Research, Report CRDC-SP-84014, (Eds.) R. L. Dimmick and M. Rausa, p. 617 (1984).

(3) Th. Herbert "Nonlinear Effects in Hydrodynamic Stability," in: AGARD Report No. 709, Special Course on Stability and Transition of Laminar Flow (1984)

(4) Th. Herbert "Highly Viscous Fluid Flow in a Spinning and Nutating Cylinder," Trans. Second Army Conference on Applied Mathematics and Computing, ARO Report 85-1 (1985).

(5) Th. Herbert "On the Viscous Roll Moment in a Spinning and Nutating Cylinder," 1984 Scientific Conference on Chemical Defense Research,

Report CRDC-SP-85006, (Ed.) Michael Rausa, p. 529 (1985). Aberdeen Proving Ground, Maryland.

(6) Th. Herbert "Viscous Fluid Motion in a Spinning and Nutating Cylinder," J. Fluid Mech., Vol. 167, pp. 181-198 (1986).

(7) Th. Herbert and R. H. Li "State Selection in Taylor-Vortex Flow," Bull. Amer. Phys. Soc. 30, p. 1689 (1985).

(8) Th. Herbert and D. Pierpont, "Visualization of the Flow in a Spinning and Nutating Cylinder," Proc. 1985 Scientific Conference on Chemical Defense Research, November 19-22, 1985, Aberdeen Proving Ground, Maryland. To appear.

The following papers are in preparation:

(9) R. H. Li and Th. Herbert, "Numerical Study of Taylor Vortex Flow" to be submitted to J. Fluid Mechanics.

(10) Th. Herbert and Stephen D. Greco, "Higher Approximations for the Viscous Flow in a Spinning and Nutating Cylinder" to be submitted to J. Fluid Mechanics.

(11) Th. Herbert and R. H. Li, "Perturbation Analysis of Taylor Vortex Flow" to be submitted to J. Computational Physics.

(12) R. H. Li and Th. Herbert "Side-Band Instability of Taylor Vortices," to be submitted to Phys. Fluids.

2. Technical Discussion

The work under this contract aimed at three major goals: (1) Reveal the origin of the despin moment that may cause severe flight instability of spin-stabilized artillery shells with liquid payloads. (2) Explore the potential of high-order perturbation methods for describing the nonlinear properties of single modes and mode interactions in hydrodynamic stability. (3) Analyze the mechanism of state selection in Taylor-Couette flow. The essentials of our efforts to achieve these goals are described in Sections 2.1 - 2.3.

2.1. The Flow in a Spinning and Nutating Cylinder

It is well-known that spin-stabilized shells carrying liquid payloads can suffer dynamical instability. For cylindrical cavities and low viscosity of the liquid, the instability due to basically inviscid inertial waves can be predicted by the Stewartson-Wedemeyer theory. This theory rests on the boundary-layer approach and is, therefore, restricted to the range of sufficiently large Reynolds numbers. The instability of certain shells like the smoke-screening projectile XM761, however, escapes such a prediction and is also distinguished in character owing to the rapid loss in spin rate. Experiments with a full-scale liquid-filled cylinder (Miller 1982) and subsequent field tests (D'Amico & Miller 1979) establish that this new flight instability is most pronounced for liquid fills of very high viscosity.

We have conducted an analysis of this problem in order to support the ongoing experiments and to independently obtain insight into the anatomy of the flow phenomena. The initial steps of this analysis were reported by Herbert (1982): evaluation of the experimental data base, dimensional analysis, scaling aspects, governing equations, and discussion of various simplifying assumptions. Two observations in this earlier work led to developing a rather successful approach. First, if the despin (negative roll) moments (Miller 1982) and void observations (Miller 1981) are correlated with the Reynolds number Re, at least three regions can be distinguished. At low Re, the despin moment increases proportional to Re, and the void in an incompletely filled cylinder is parallel to the spin axis. This suggests a simple fluid motion that is essentially independent of the axial coordinate, except in the neighborhood of the end walls. In a middle range of Re, the despin moment assumes a maximum, and a wavy distortion of the void seems to indicate a cellular structure of the fluid motion. This cellular motion can, in principle, originate from hydrodynamic instability of the basic flow with respect to axially periodic disturbances. At still higher Reynolds numbers, the despin moment decreases with increasing Re in a manner not clearly defined by the few available data points. The void observations indicate, however, that the motion ultimately becomes turbulent.

The second observation is the appearance of the nutation rate and angle as a small parameter in the equations for the deviation from solid-body rotation. The forcing term due to nutation can be considered small enough for linearization of the equations in the situations of practical interest.

Consequently, our research focused on three topics. First, we performed a theoretical analysis of "simple" fluid motions at low Reynolds number that satisfied the linearized equations for the deviation from rigid body rotation. Second, we designed a small-scale, low-cost experiment for visualization of the interior fluid motion. The results of these efforts are discussed in sections 2.1.1 and 2.1.2, respectively. Third, the work on the "simple" fluid motion stimulated and guided the development of a spectral code for solving the Navier-Stokes equations in a finite cylinder. This ongoing effort is described in Section 2.1.3.

2.1.1 The Deviation from Solid Body Rotation

A formal analysis of the equations† for the deviation of the velocity field from solid body rotation suggests that (1) the equations can be linearized without introducing major errors, (2) at low Reynolds numbers Re *, the velocity field is independent of the axial direction over a considerable part of the relatively long ($\gamma = 4.3$) cylinder, and (3) the flow is essentially in the axial direction and turns at the ends. Application of these conceptual assumptions turned out very fruitful. A detailed description of the results and comparison with computational and experimental data is given in the paper "Viscous Fluid Motion in a Spinning and Nutating Cylinder" (Appendix A), that will soon appear in the Journal of Fluid Mechanics (Herbert 1986). Here, we report only the main conclusions.

The model of a two-dimensional unidirectional flow in a finite segment of an infinite cylinder yields the solution of the linearized equations in analytical form. The disregard of the end walls has some obvious consequences: the turning flow near the ends and the associated contributions of pressure and shear stresses to the moments cannot be obtained from this model. Nevertheless, we gather understanding as well as quantitative information. The velocity field of the core flow

† Detailed equations are given in Appendix A.

* We use the notation introduced in Appendix A.

agrees well with computational results (Vaughn et al. 1983, 1985) for low Reynolds numbers. The analytical result is an evident example for the formation of boundary layers. The core flow can be utilized as a basic flow in studies of hydrodynamic instability with respect to cellular motions. The parametric excitation of such cells by the azimuthally periodic deviation has been discussed by Herbert (1985a). The core flow also represents the lowest-order approximation to the solution of the nonlinear equations and can be extended by higher-order terms.

The roll moment agrees well with measured and computed values and can also be found at Reynolds numbers too large for successful numerical simulations. The roll moment originates from Coriolis forces. While the direct calculation of the yaw moment suffers from neglecting the pressure contribution, the yaw moment can be found from the roll moment using the relations given by Murphy (1984, 1985). The pitch moment remains an open issue. The average rate of change of temperature is found to be proportional to roll moment and spin rate. This estimate needs further verification once more experimental data become available.

The simple form and scaling relations of our results provide guidance for sorting and evaluating the experimental data base. The results also suggest various improvements in the experimental procedures. First, the changes in temperature and viscosity should be carefully monitored. With the effective viscosity known, a closer agreement between theory and observation is to be expected. Second, the yet neglected variation of the roll moment with the spin rate is considered relevant and in fact provides the roll moment in some range of Reynolds numbers. Instead of recording the roll moment as a function of Re by using numerous viscosities at fixed spin rate, very similar data can be generated by varying the spin rate for a few fluids. For directing the research efforts within this project, it has been most revealing that the characteristic variation of roll moment versus Reynolds number, in particular the sharp maximum at $Re \approx 19$, is a property of the unidirectional model flow. This result contradicted the earlier working hypothesis which attributed the occurrence of this maximum to hydrodynamic instability and the onset of cellular motions.

Recently, we have extended the analysis of the flow in an infinitely long cylinder to account for nonlinearity by using a perturbation method. The equations up to the third order were solved partly with analytical, partly with numerical (spectral) methods. The second order solution provides azimuthal and radial velocity components in agreement with computational results. The aperiodic component of the azimuthal velocity causes the shear stress on the wall that tends to despin the cylinder. The second-order terms have no effect on the despin moment derived at lower order. The third-order correction to the moments is very small, and can be neglected for practical purpose. The results of the perturbation analysis indicate that there is little difference between the velocities governed by the linear and nonlinear system. This fact is important for the design of efficient spectral solvers. The analytical results provide a simple mean for estimating the number of expansion functions needed in the azimuthal and radial directions.

2.1.2 Flow Visualization

Although theoretical (Herbert, Appendix A) and computational (Vaughn et al. 1985) work provides some insight into the interior fluid motion, the nature of the phenomena remains largely in the dark. This is especially true for the range of medium and high Reynolds numbers where finite-amplitude cellular motions and ultimately turbulence are expected to occur. This range is barely within the scope of computational methods, nor can it be fully explored with the theoretical means of sections 2.1.1.

Previous experiments (Miller 1981) using a partially filled full-scale cylinder revealed some axial nonuniformity of the flow at higher Re without showing details of the flow field. Later attempts to use flow tracers (Miller & Oberkampf, personal communication) had little success due to the high spin rates (accelerations) combined with minute density differences between working fluid and tracer particles. Even carefully centrifuged and selected particles failed to follow the liquid path, probably due to changes of temperature during the run. Attempts to employ laser-induced fluorescence (Miller 1985) were partly successful after changing the time scale, i.e. to lower spin rate, nutation rate, and viscosity at fixed values of the dimensionless parameters. These efforts have been

discontinued, however, due to continuing lighting problems.

Evaluation of the experimental attempts to visualize the fluid flow clearly reveals the extreme full-scale conditions as evil. Conclusive experiments can be conducted by exploiting the principals of dynamical similarity and appropriate scaling laws. These aspects have been discussed in earlier work (Herbert 1982) and extended by the analysis in Appendix A.

A description of our experimental setup, the visualization technique, and some results are given in Appendix B. More details are provided in the Senior Project Report by D. Pierpont (1985).

The experimental effort has clearly shown the feasibility of flow visualization with relatively simple means. The numerous photographs obtained reveal the basic pattern of the flow and the changes of the flow structure as the Reynolds number increases. Perhaps the most striking result of this visual study is the manifold of patterns at higher Reynolds numbers that has not been revealed by the computational work. The study also has suggested improvements in the experimental setup and procedures that would enhance the quality of the results. An exploratory study has indicated that an improved test fixture with proper timing devices would also allow for laser-Doppler velocimetry. In this way, data for verification of computer solutions could be obtained.

2.1.3 Spectral Navier-Stokes Solver

Two independent efforts have provided codes for finding the steady solution to the Navier-Stokes equations in a finite cylinder. Vaughn et al. (1983, 1985) introduced artificial time-dependence by Chorin's method and used finite differences in space and time. The code is rather demanding in terms of computer time due to the large number of time steps required for convergence. A direct approach to the steady solution has been implemented by Nagel & Strikwerda (1984) using a pseudospectral method for the azimuthal, finite differences in all other variables. Details on the potential of this code have not yet been published. Both codes, however, are known to be deficient at large Reynolds numbers and demanding in terms of computer time. Guided by our analytical work, we are in the process of developing a fully spectral (collocation)

approach to the steady problem with Fourier series in azimuthal (ϕ) and Chebyshev series in radial (r) and axial (z) direction. With N_r, N_ϕ, and N_z collocation points in the spatial variables, a straightforward approach in the $N_v = 4$ natural variables leads to an algebraic system of dimension $N = N_v \cdot N_r \cdot N_\phi \cdot N_z$. The resolution of the code of Vaughn et al. can be matched with a matrix size that can be handled with desk-top computers (e.g. Apollo DN300, DN3000 or Sun). The task can be simplified by (1) exploiting symmetry of the motion, (2) reducing and splitting the number of variables, e.g. into $N_v = 3$ vorticity components plus $N_r = 1$ pressure, or (3) utilizing divergence-free expansion functions (Leonard 1981, Leonard & Wray 1982). At present, we have successfully used two codes (without and with exploiting symmetry) in all four natural variables. These codes provide accurate velocity components resulting from the linear or nonlinear system of equations. Samples of the velocity field near the Reynolds number of maximum despin are shown in Figures 1-5. Comparison of Figures 1 and 2 indicates the small effect of nonlinearity. The further development was slowed down by the occurrence of a spurious pressure term due to the lack of non-redundant conditions along the joint between cylindrical sidewalls and the end plates. We have attempted a solution of this (known) problem by studying a two-dimensional analogon, the flow in a square under a given force field. The study has just been completed. Continuation of this work is supported by the Army AMCCOM under Contract DAAK11-83-K-0011.

2.2 Analysis and Improvement of Perturbation Series

The use of perturbation expansions is the foundation of the weakly nonlinear stability theory. With very few exceptions, research in this framework has only considered the lowest-order nonlinear correction to the results of linear stability theory. Often, however, these weakly nonlinear results are used at definitely finite values of the perturbation parameter given e.g. by experimental data. The questions that arise are whether these physical values are "sufficiently small," and whether the low truncation provides a reasonable approximation. In mathematical terms, these questions are whether the series is used within the radius of convergence and how large the truncation error is.

A second problem area in the weakly nonlinear stability theory concerns the relevance and completeness of multi-mode models for the analysis of nonlinear interactions. Numerous such models have been suggested and studied. They failed, however, to provide reliable qualitative and quantitative information on the physical phenomena under consideration.

The aim of our work has been to extend perturbation series to higher order, to analyze their radius of convergence and the nature of the singularity nearest to the origin, and to recast the series in other forms in order to extend the radius and improve the rate of convergence. As prototype problems, we have chosen various topics related to the stability of plane Poiseuille flow and circular Couette flow. The results for circular Couette flow are given in the Ph.D. thesis of R. H. Li. Detailed results for plane Poiseuille flow will be reported in the forthcoming Ph.D. thesis of K. Sethuramalingam.

2.2.1 High-Order Expansions for Single Modes

It has been shown by Herbert (1980) that the construction of high-order Landau series is just a matter of computer time once a rational formulation of the problem has been found. In a rather general way, a rational formulation of the nonlinear stability problem for single TS-modes in plane Poiseuille flow has been given by Herbert (1983). The results for this case can be easily checked by comparison with data obtained from using the concept of harmonic balance in combination with an arc-length continuation method (Herbert 1978).

Computer programs for constructing high-order series have been provided with restrictions on the maximum order by computer time and/or memory only. Parameter expansions (in Reynolds number or wavenumber) and two types of coordinate expansions (Herbert 1983) have been implemented. Given the expansion coefficients, numerous techniques for analyzing and improving the convergence of perturbation series (VanDyke 1984) have been explored. For plane Poiseuille flow, the constraint on the radius of convergence arises from a branch cut caused by a non-physical solution at negative disturbance energy. Although properties of this nearest singularity can be analyzed in detail, it has not been possible to remove or displace this singularity. Application of Padé approximants

nevertheless provides accurate results at amplitudes up to 15%, far beyond the physically relevant range, while the original series has a comparable rate of convergence at amplitudes less than 2%.

For Taylor vortices in circular Couette flow, accurate results can be obtained at sufficiently small supercritical Taylor numbers and wavenumbers larger than the critical value. At low wavenumbers, the single-mode expansion fails due to resonance in the perturbation equations and the occurrence of secular terms. This failure has led to the development of a two-mode model that reveals the interesting phenomenon of a changeover from low wavenumber disturbances to Taylor vortices of twice this wavenumber. At higher Taylor numbers, the radius of convergence of the single-mode series is limited by a physical branch cut. The origin of this singularity depends on the type of expansion. In coordinate (time) expansions, the cause is an overshoot of the amplitude and an oscillatory approach to the equilibrium value. In parameter expansions for equilibrium states, the branch cut reflects a maximum of the equilibrium amplitude. Although Padé approximants can be used to continue the solution beyond branch cuts, their convergence deteriorates. Attempts to recast the series in terms of curvature versus arc length were partially successful. However, this procedure is very sensitive to round-off or truncation errors.

2.2.2 Interacting Modes: Weakly Nonlinear Models

The evaluation of weakly nonlinear models was conducted in parallel with an analysis of secondary instability using Floquet systems of disturbance equations (Herbert 1984). The development of the Floquet analysis was supported by the National Science Foundation. As a prototype for both approaches, we choose plane Poiseuille flow.

We have concentrated our efforts on the Benney-Lin model (Benney & Lin 1960), Craik's resonant triad (Craik 1971), and the model of parametric excitation of streamwise vortices by two-dimensional waves (Herbert & Morkovin 1980). As a general conclusion, the use of high-order expansions for multi-mode interactions was found very demanding in terms of computer time and storage. Moreover, we were not able to quantitatively reproduce the observations.

The Benney-Lin model considers the interaction between a two-dimensional wave and oblique waves of arbitrary spanwise wavelength. In the light of resonant wave interaction, the question of synchronization has created much interest. In contrast to previous investigations, we found that nonlinear synchronization can occur at reasonable amplitudes. The relevance of this model to peak-valley splitting in plane Poiseuille flow, however, cannot be assured. Results of the Floquet analysis clearly reveal that the principal mode of three-dimensional instability does not originate from a Benney-Lin type interaction.

Craik's model of a resonant triad of a two-dimensional wave with subharmonic oblique waves of a specific spanwise wavelength has been found to be relevant in boundary layer transition. In plane Poiseuille flow, this mechanism is inactive by reasons of symmetry. Floquet analysis has shown that subharmonic three-dimensional instability in plane Poiseuille flow originates from a near-resonant triad between modes of Squire's equation. These modes have been disregarded in all weakly nonlinear theories.

The model of parametric excitation of longitudinal vortices by two-dimensional waves reveals some pitfalls of weakly nonlinear modeling. Reasonable results are obtained only in some range of the spanwise wavelength. For large wavelength, the results suffer from the low order of truncation. For small wavelength, the results suffer from the incompleteness of the model.

2.2.3 Floquet Analysis of Secondary Instability

In this approach, it is recognized that primary instability with respect to spatially periodic disturbances causes the original basic flow to be modulated e.g. by a Taylor vortex or TS wave of small but finite amplitude. In shear flows, the local flow can be considered as streamwise periodic in a frame moving with the phase velocity. It was suggested (Herbert & Morkovin 1980) that such periodic modulation of the flow may cause parametric excitation of secondary instability. This secondary instability is a new linear mechanism and is governed by a Floquet system of disturbance equations with periodic coefficients. The main problems then are to identify classes and forms of solutions from known mathematical properties of such systems and to solve the resulting high-order systems of

ordinary differential equations. All results for plane Poiseuille flow and Blasius boundary layer flow yet obtained are consistent and in good quantitative agreement with experimental data.

A comprehensive survey on the development and application of this approach (Herbert 1985b) has been given as an invited lecture at the Second IUTAM Symposium "Laminar-Turbulent Transition," July 9-13, 1984, Novosibirsk, USSR.

2.3 Analysis of Taylor-Vortex Flow

The flow between coaxial rotating cylinders is one of the basic problems in nonlinear hydrodynamic stability theory and one of the fluid mechanical models for the cascade of bifurcations into chaotic motion. Certain puzzling features, however, occur near the first bifurcation of circular Couette flow into Taylor-vortex flow. In contrast to the wide region of wavenumbers β for which linear stability theory predicts instability, experiments can obtain Taylor-vortex flow only in a surprisingly small region of wavenumbers near the critical value β_{cr}. We have used various perturbation methods and a numerical method in order to analyze the properties of finite-amplitude Taylor vortices and the mechanism of wavenumber selection. Both the evolution and the steady state of the flow originating from single or a discrete spectrum of disturbances were studied. The results of this study are reported in the Ph.D. thesis of R. H. Li. A series of papers for archival publication are in preparation. The results of perturbation methods for single-mode expansions are summarized in Section 2.2.1 above.

2.3.1 Sideband instability.

It is common to attribute the small band of observable Taylor vortices to a sideband instability (DiPrima & Swinney 1985). The original analysis of this mechanism in the neighborhood of the critical point by Kogelman & DiPrima (1970) reduced the wavenumber band of stable Taylor vortices to $1/\sqrt{3}$ times the baud predicted by the linear theory to both sides of β_{cr}. Nakaya (1974) performed an analysis of this problem taking fifth-order terms into account. His results seem to indicate that higher-order terms tend to reduce the band of

stable, observable Taylor vortices. We have, therefore, used high-order parameter and coordinate expansions in order to establish the region of stable Taylor vortices. In contrast to Nakaya, we find little effect of the high-order terms on the Kogelman-DiPrima result. Since we applied two different methods to arrive at this conclusion and because other studies revealed additional support, we consider Nakaya's results to be wrong and misleading as to the cause of the small band of stable Taylor vortices.

2.3.2 Two-mode models of Taylor vortices.

One of the outcomes of the study on side-band instability was the occurrence of a singularity in the third-order Landau constant. This singularity originates from resonance in the perturbation equations for the harmonic with wavenumber 2β if the Taylor number is large enough for modes with β and 2β to be inside the unstable domain. The occurrence of the resulting secular terms can only be removed by introducing a second mode of wavenumber 2β, and to consider a set of two coupled Landau equations. Evaluation of this two-mode model clearly revealed that the growth of linear Taylor-vortex modes with small wavenumbers β does not lead to an equilibrium Taylor vortex at this wavenumber. Instead, energy is transferred into the harmonic with 2β. This means that the common picture of a neutral surface of stable equilibrium Taylor vortices in the full linearly unstable region does not hold up. Taylor vortices of finite amplitude do not exist at small wavenumbers. This finding is consistent with the results recently reported by Keller & Meyer-Spasche (1985).

An extension of our two-mode model for the interaction of modes with wavenumbers $n\beta$ and $(n+1)\beta$ also show that Taylor vortices at large wavenumbers tend to be unstable in the presence of low-wavenumber components, and evolve into vortices of a wavenumber as close as possible to β_{cr}.

The two-mode models provide useful information on stable and unstable equilibrium solutions and predict a band of stable Taylor vortices consistent with, but smaller than that obtained from the sideband instability mechanism. The results are not satisfactory throughout, however, since solutions at larger Taylor numbers and amplitudes suffer from the overshoot singularity (see Section 2.2.1).

Moreover, the perturbation method is invalid for small values of β that are located in the linearly stable domain (Herbert 1983). It was, therefore, decided to complement our study by the analysis of the temporal development of Taylor vortices from various initial conditions using a numerical scheme.

2.3.3 Numerical studies.

The numerical method uses spectral collocation with Chebyshev polynomials in the radial direction, finite differences in time, and solves the coupled system of equations for Fourier modes of wavenumbers $\beta_n = n\,\Delta\beta$, $n = 0, \cdots N$, in the axial direction. The value of N depends on the special application, especially on the value of $\Delta\beta$, and may be $N = 50$ or even larger. The detailed knowledge of the eigenvalue spectrum of the linear problem has been very useful in designing the implicit scheme. Accurate and reliable operation for the nonlinear problem has been secured by numerical experimentation.

Application of the numerical method to a single small initial disturbance of wavenumber β_1 verifies the results of the perturbation methods. Disregarding the sideband instability mechanism, Taylor vortices of finite equilibrium amplitude can exist only in the unstable domain if β_1 is sufficiently large. For smaller wavenumbers, the flow selects a Taylor vortex of wavenumber β_n with n such that β_n is as close as possible to β_{cr}. It is interesting to note that disturbances with β_1 in the stable domain initially decay. Their harmonics, however, lead to the development of Taylor vortices of appropriate wavenumber β_n near β_{cr}. This result suggests a revised view of the role of linearly stable modes in a nonlinear framework.

Analysis of more complicated initial data shows that the development is characterized by only a few patterns of behavior. One of these is essentially the same as for single input modes. The most interesting behavior, however, starts with the development of a finite amplitude Taylor vortex at relatively large β_n into a virtual equilibrium that may last for a long time. In the presence of a disturbance of sufficiently small wavenumber β_1 and arbitrarily small amplitude, this Taylor vortex is ultimately destroyed and replaced by a vortex of wavenumber β_m near β_{cr}. The width of the band of stable vortices near β_{cr} is

directly related to the lowest wavenumber β. Considered the finite length of cylinders used in experiments and the presence of a large disturbance of circular Couette flow caused by the cylinder ends, we find a direct relation between the baud width of observable Taylor vortices and the smallest wavenumber possible for a given length experiment. One may suspect that the Taylor flow in infinite cylinders at fixed Taylor number is unique.

ACKNOWLEDGMENT

The open cooperation and sharing of data with Miles C. Miller (CRDC) and Harold R. Vaughn (Sandia Laboratories) are greatly appreciated.

REFERENCES

1. D. J. Benney and C. C. Lin 1960 "On the secondary motion induced by oscillations in a shear flow," *Phys. Fluids*, vol. 3, pp. 656-657.

2. A. D. D. Craik 1971 "Nonlinear resonant instability in boundary layers," *J. Fluid Mech.*, vol. 50, pp. 393-413.

3. W. P. D'Amico and M. C. Miller 1979 "Flight Instability produced by a rapidly spinning, highly viscous liquid," *J. Spacecraft and Rockets*, vol. 16, pp. 62-64.

4. R. C. DiPrima and H. L. Swinney 1985 "Instabilities and transition in flow between concentric rotating cylinders," *Topics in Applied Physics*, vol. 45, pp. 140-180, Springer-Verlag.

5. Th. Herbert 1978 "Die neutrale Fläche der ebenen Poiseuille-Strömung," Habilitationsschrift, Universität Stuttgart.

6. Th. Herbert 1980 "Nonlinear stability of parallel flows by high-order amplitude expansions," *AIAA J.*, vol. 18, pp. 243-247.

7. Th. Herbert 1982 "Fluid motion in a rotating and nutating cylinder - Part I," Report prepared under the Scientific Services Program. Published as Report CRDC-CR-84087 (1984)..

8. Th. Herbert 1983 "On perturbation methods in nonlinear stability theory," *J. Fluid Mech.*, vol. 126, pp. 167-186.

9. Th. Herbert 1984 "Modes of secondary instability in plane Poiseuille flow," in *Turbulence and Chaotic Phenomena in Fluids*, ed. T. Tatsumi, pp. 53-58, North-Holland.

10. Th. Herbert 1985a "Highly viscous fluid flow in a spinning and nutating cylinder," Trans. Second Army Conference on Applied Mathematics and Computing, pp. 883-893, ARO Report 85-1.

11. Th. Herbert 1985b "Secondary instability of plane shear flows - theory and applications," in *Laminar-Turbulent Transition*, ed. V. V. Kozlov, pp. 9-20, Springer-Verlag.

12. Th. Herbert 1986 "Viscous fluid motion in a spinning and nutating cylinder," *J. Fluid Mech.*, vol. 167, pp. 181-198.

13. Th. Herbert and M. V. Morkovin 1980 "Dialogue on bridging some gaps in stability and transition research," in *Laminar-Turbulent Transition*, ed. R. Eppler and H. Fasel, pp. 47-72, Springer-Verlag.

14. S. Kogelman and R. C. DiPrima 1970 "Stability of spatially periodic supercritical flows in hydrodynamics," *Phys. Fluids*, vol. 13, pp. 1-11.

15. A. Leonard 1981 "Divergence-free vector expansions for 3-D flow simulations," *Bull. Amer. Phys. Soc.*, vol. 26, p. 1247.

16. A. Leonard and A. Wray 1982 "A numerical method for the simulation of three-dimensional flow in a pipe," in *Proc. 8th Int. Conf. Num. Meth. in Fluid Dyn., Aachen, Germany*, ed. E. Krause.

17. R. Meyer-Spasche and H. B. Keller 1985 "Some bifurcation diagrams for Taylor vortex flows," *Phys. Fluids*, vol. 28, pp. 1248-1252.

18. M. C. Miller 1981 "Void characteristics of a liquid filled cylinder undergoing spinning and coning motion," *J. Spacecraft and Rockets*, vol. 18, pp. 286-288.

19. M. C. Miller 1982 "Flight instabilities of spinning projectiles having nonrigid payloads," *J. Guidance, Control, and Dynamics*, vol. 5, pp. 151-157.

20. M. C. Miller 1985 "Visualization studies of viscous liquid flow in a spinning and coning cylinder," in *Proc. 1984 Scientific Conf. on Chemical Defense Research, Aberdeen Proving Ground, Maryland*, ed. M. Rausa, pp. 541-546, Report CRDC-SP-85006.

21. C. M. Murphy 1984 "A relationship between liquid roll moment and liquid side moment," BRL Memorandum Report ARBRL-MR-03347.

22. C. M. Murphy 1985 "A relation between liquid roll moment and liquid side moment," *J. Guidance, Control, and Dynamics*, vol. 8, pp. 287-288.

23. C. Nakaya 1974 "Domain of stable periodic vortex flows in a viscous fluid between concentric circular cylinders," *J. Phys. Soc.*, vol. 36, pp. 1164-1173.

24. J. C. Strikwerda and Y. M. Nagel 1985 "A numerical method for computing the flow in rotating and coning fluid-filled sylinders," in *Proc. 1984 Scientific Conference on Chemical Defense Research, Aberdeen Proving Ground, Maryland*, ed. M. Rausa, pp. 523-527, CRDC-SP-85006.

25. M. VanDyke 1984 "Computer-extended series," *Ann. Rev. Fluid Mech.*, vol. 16, pp. 287-309.

26. H. R. Vaughn, W. L. Oberkampf, and W. P. Wolfe 1983 "Numerical solution for a spinning nutating fluid-filled cylinder," Sandia Report SAND 83-1789.

27. H. R. Vaughn, W. L. Oberkampf, and W. P. Wolfe 1985 "Fluid motion inside a spinning nutating cylinder," *J. Fluid Mech.*, vol. 150, pp. 121-138.

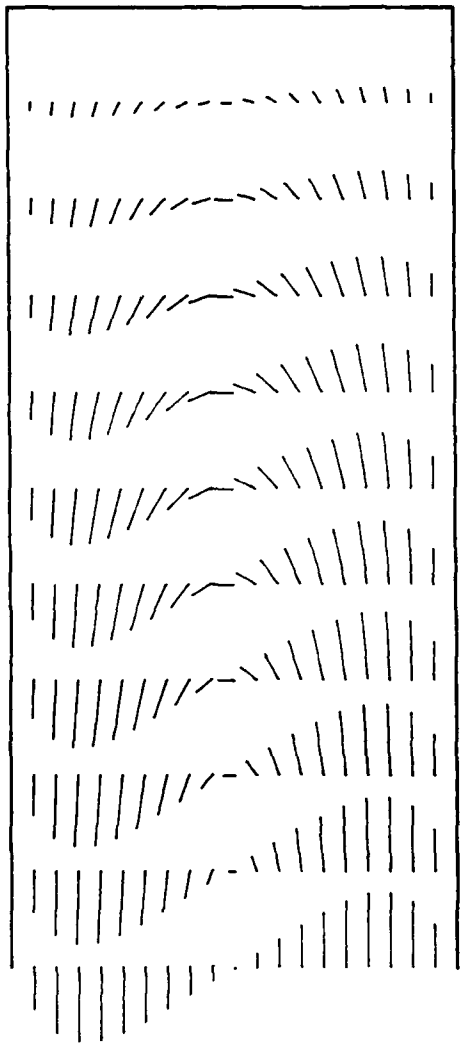

Figure 1. Vector plot of the radial and axial velocities in the plane of the spin and nutation axes ($\phi = 0$) based on equations linearized in ϵ.

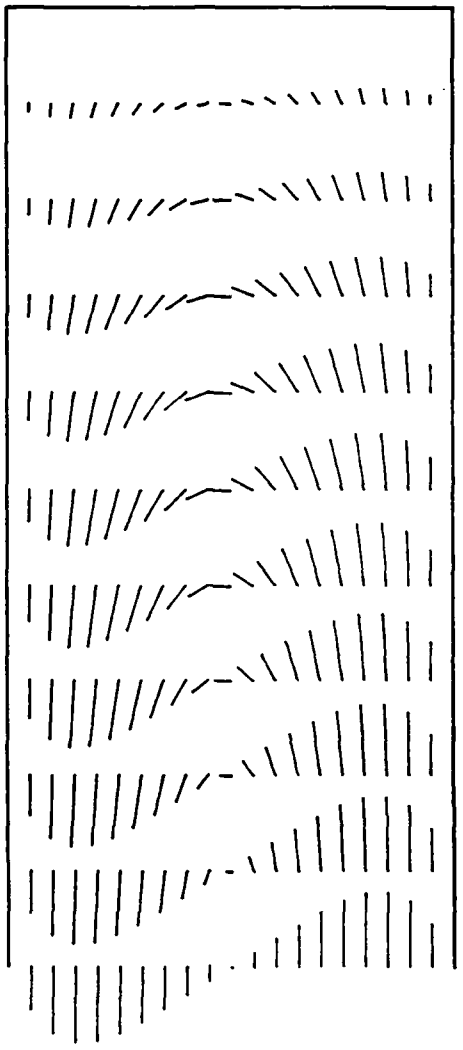

Figure 2. Vector plot of the radial and axial velocities in the plane of the spin and nutation axes ($\phi = 0$) based on the non-linear equations.

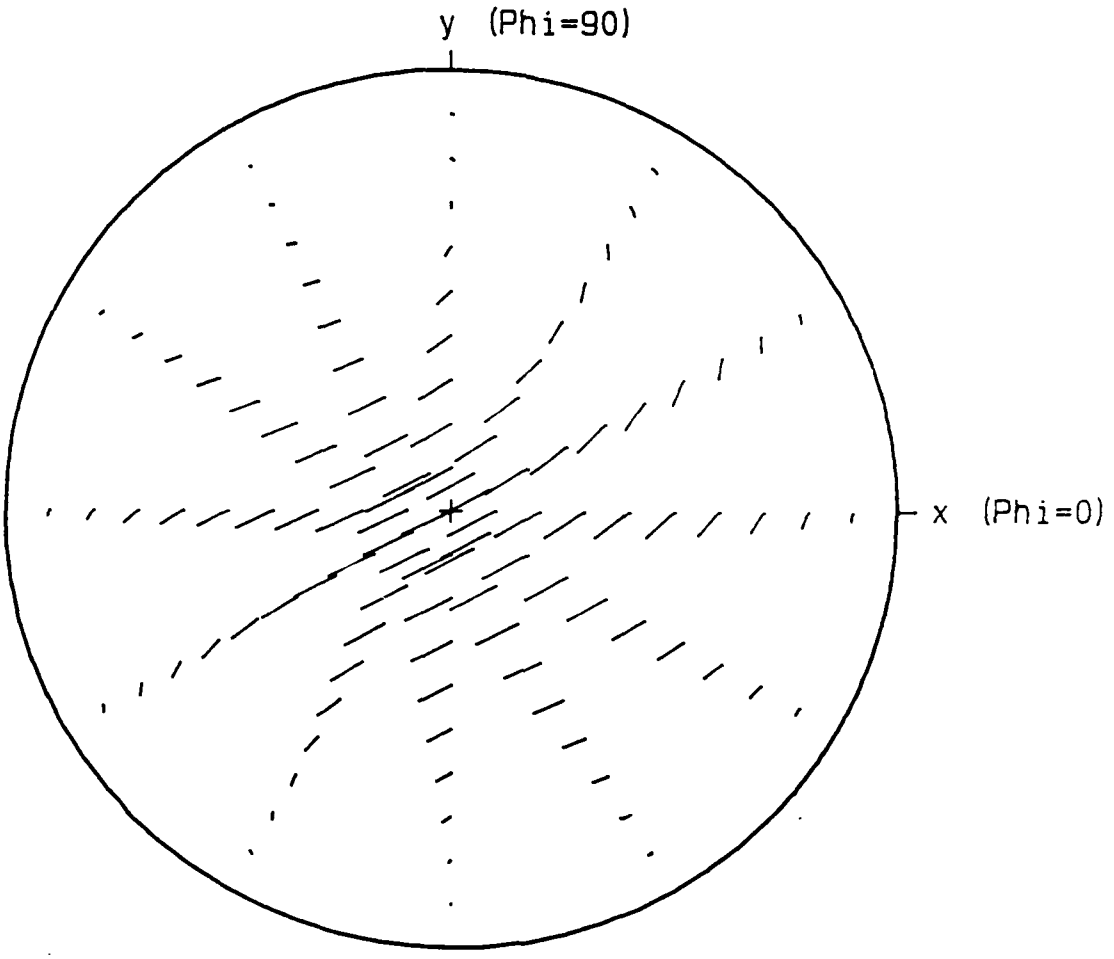

Figure 3. Vector plot of the radial and azimuthal velocities in the cross section at $z = 0.9$ times the half-length c of the cylinder.

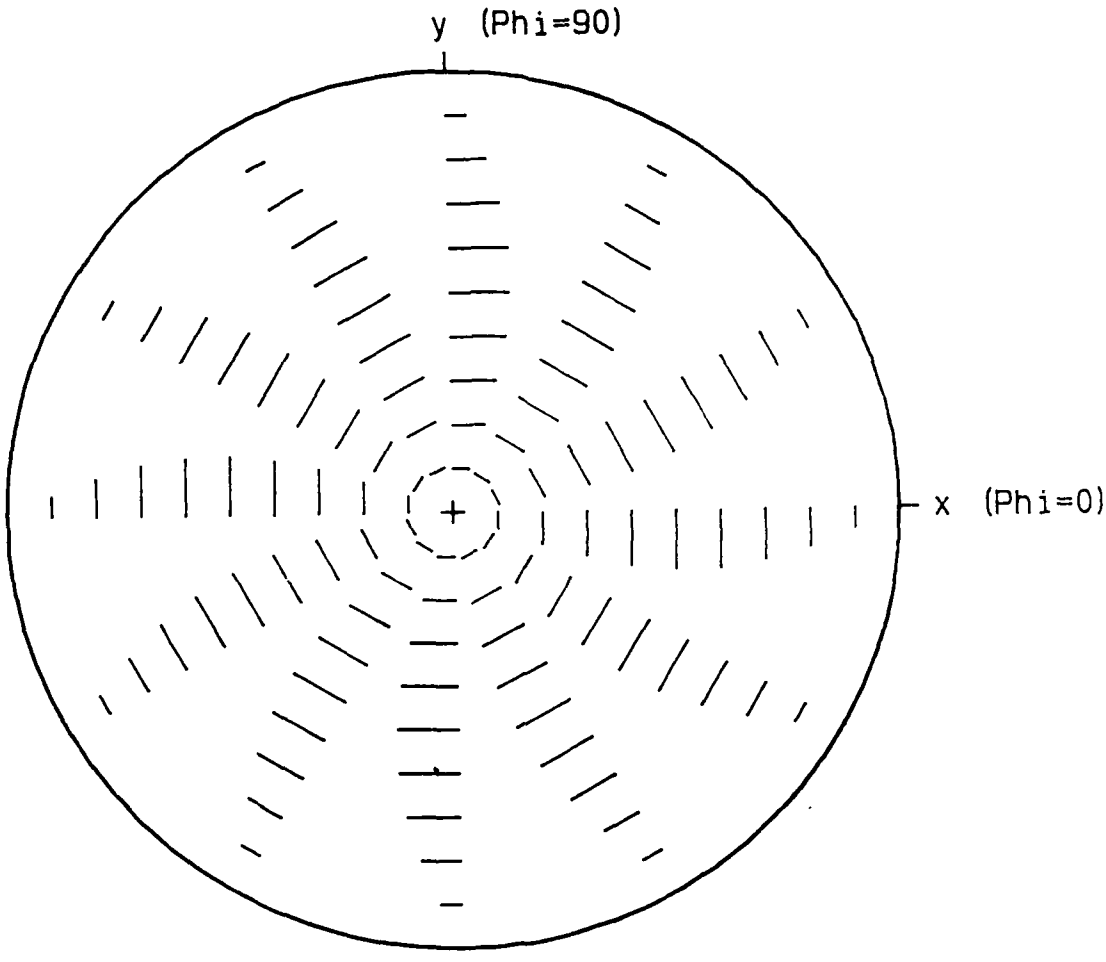

Figure 4. Vector plot of the radial and azimuthal velocities in the center cross section, $z = 0$, of the cylinder. The shear exerted by this almost aperiodic velocity tends to despin the cylinder.

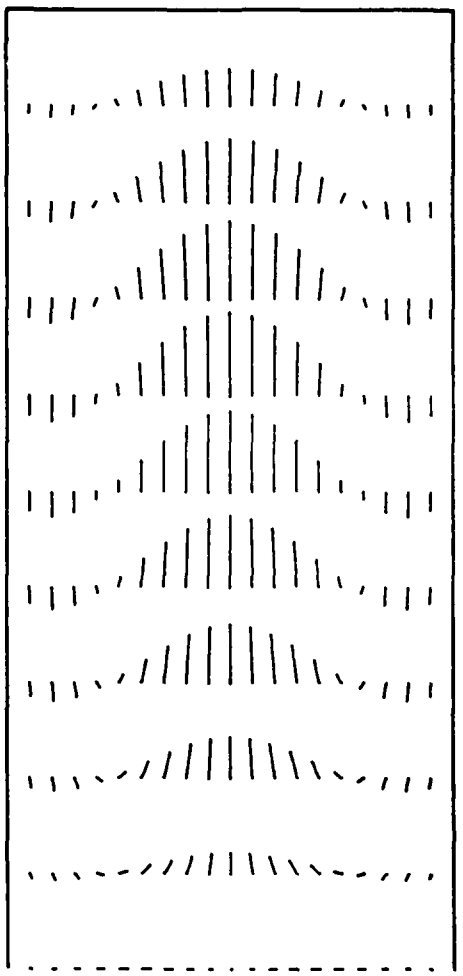

Figure 5. Vector plot of the mean velocities in the radial and axial directions. The symmetry and circulatory pattern of this mean flow is consistent with the results of flow visualizations at low Reynolds number (Appendix B, Fig. 2, 3).

Appendix A

Viscous Fluid Motion in a Spinning and Nutating Cylinder

by

Thorwald Herbert

Department of Engineering Science and Mechanics
Virginia Polytechnic Institute and State University
Blacksburg, Virginia 24061

To appear in:

Journal of Fluid Mechanics
Vol. 167, pp. 181-198 (1986)

ABSTRACT

Spin-stabilized projectiles with liquid payloads can experience a severe flight instability characterized by a rapid yaw-angle growth and a simultaneous loss in spin rate. Laboratory experiments and field tests have shown that this instability originates from the internal fluid motion in the range of high viscosity. After evaluation of the experimental data and analysis of the equations for the fluid motion in a spinning and nutating cylinder, we have developed a simple model of this flow. Disregarding the finite length of the cylinder, this model provides the flow field and the viscous contribution to the liquid moments in analytical form. At low Reynolds number, the flow field agrees well with computational results for the center section of a cylinder of aspect ratio 4.3. The roll moment caused by this flow largely agrees with experimental data for a wide range of Reynolds numbers. Estimates of the temperature variation indicate that discrepancies at very low Reynolds numbers may originate from associated changes of the viscosity during the experiments.

1. Introduction

It is well-known that spin-stabilized shells carrying liquid payloads can suffer dynamical instability. For cylindrical cavities and low viscosity of the liquid, the instability due to basically inviscid inertial waves can be predicted by the Stewartson-Wedemeyer theory (Stewartson 1959; Wedemeyer 1966). This theory rests on the boundary-layer approach and is, therefore, restricted to the range of sufficiently large Reynolds numbers. The instability of certain shells like the XM761 (D'Amico 1977; 1978), however, escapes such a prediction and is also distinguished in character owing to the rapid loss in spin rate. Experiments with a full-scale liquid-filled cylinder (Miller 1982) and subsequent field tests (D'Amico & Miller 1979) establish that this new flight instability is most pronounced for liquid fills of very high viscosity.

We conduct a theoretical analysis of this problem in order to support the ongoing experiments and to independently obtain insight into the anatomy of the flow phenomena. The initial steps of this analysis are reported elsewhere (Herbert 1982): evaluation of the experimental data base, dimensional analysis, scaling aspects, governing equations, and discussion of various simplifying assumptions. Two observations in this earlier work led to the approach discussed in the following. First, if the despin (negative roll) moments (Miller 1982) and void observations (Miller 1981) are correlated with the Reynolds number Re, at least three regions can be distinguished. At low Re, the despin moment increases proportional to Re, and the void in an incompletely filled cylinder is parallel to the spin axis. This suggests a simple fluid motion that is essentially independent of the axial coordinate, except in the neighborhood of the end walls. In a middle range of Re, the despin moment assumes a maximum, and a wavy distortion of the void seems to indicate a cellular structure of the fluid motion. This cellular motion can, in principle, originate from hydrodynamic instability of the basic flow with respect to axially periodic disturbances. At still higher Reynolds numbers, the despin moment decreases with increasing Re in a manner not clearly defined by the few available data points. The void observations indicate, however, that the motion ultimately becomes turbulent.

The second observation is the appearance of the nutation rate and angle as a small parameter in the equations for the deviation from solid-body rotation. The forcing term due to nutation can be considered small enough for linearization of the equations in the situations of practical interest.

In the following, we describe the development of a simple system of equations for the basic flow. Analytical solutions are given for the flow field, for the liquid moments, and for the

rate of change of temperature. A comparison is made with computer simulations of the flow (Vaughn et al. 1983; 1985) and with experimental data for the moments (Miller 1982).

2. Governing Equations

We consider the motion of a fluid of density ρ and viscosity μ in a cylinder of radius a and length $2c$ that rotates with the spin rate ω about its axis of symmetry, the z-axis. We consider the motion with respect to the nutating coordinate system x,y,z. This system is obtained from the inertial system X,Y,Z, by a rotation with the nutation angle θ about the axis $Y=y$. Therefore, x is in the Z,z-plane, and this plane rotates about the Z-axis with the nutation rate Ω. The two axes of rotation intersect in the center of mass of the cylinder, as shown in figure 1. We consider $\omega>0$, Ω, and $0\leq\theta\leq\pi/2$ as constant. This is in some contrast to the experimental procedures for measuring the despin moment (Miller 1982). In these experiments, the apparatus is held at constant conditions until a steady (or quasisteady) flow is established. After shut-down of the spin drive, the decrease of ω as a function of time is recorded in order to obtain the roll moment.

The fluid motion is governed by the Navier-Stokes equations written in the nutating coordinate system:

$$\rho[\frac{D\mathbf{V}_n}{Dt} + 2\mathbf{\Omega} \times \mathbf{V}_n + \mathbf{\Omega} \times (\mathbf{\Omega} \times \mathbf{r})] = -\nabla P_n + \mu\nabla^2\mathbf{V}_n \,, \tag{1a}$$

$$\nabla\cdot\mathbf{V}_n = 0 \,. \tag{1b}$$

$\mathbf{V}_n$ is the velocity measured in the nutating frame, P_n the pressure, and $\mathbf{r}$ the position vector. The body force due to gravity has been disregarded. Equations (1) are subject to the no-slip and no-penetration conditions at the cylinder walls.

It is convenient (Herbert 1982) to split the velocity and pressure fields according to

$$\mathbf{V}_n = \mathbf{V}_s + \mathbf{V}_d \,, \quad P_n = P_s + P_d \,, \tag{2}$$

where $\mathbf{V}_s, P_s$ describe the state of pure solid body rotation, whereas $\mathbf{V}_d, P_d$ represent the deviation from solid body rotation. The advantage of this isolated view on the deviation is obvious:

$\mathbf{V}_d$ and the reduced pressure P_d are responsible for the observed flight instability. A glance at the equations shows that $V_d \equiv 0$ and $P_d \equiv 0$ if either one of the following conditions is satisfied: $\omega = 0$, $\Omega = 0$, $\theta = 0$ or $\mu \to \infty$ (solid fill).

The equations for $\mathbf{V}_d$,P_d are written in terms of nondimensional quantities $\mathbf{v}_d$,p_d. We use a,ω, and ρ for scaling length, time and mass. Note that this choice is ambiguous (Herbert 1982) and excludes the case ω=0 which lacks practical interest. The problem then depends on four nondimensional parameters:

$\lambda = c/a$	aspect ratio
θ	nutation angle
$\tau = \Omega/\omega$	frequency
$Re = \rho\omega a^2/\mu$	Reynolds number.

The aspect ratio enters the solution only through the boundary conditions. The boundary conditions on $\mathbf{v}_d$ are homogeneous.

In cylindrical coordinates r,ϕ,z, the equations for the nondimensional deviation velocity $\mathbf{v}_d = (v_r, v_\phi, v_z)$ and pressure p_d take the form

$$\frac{1}{r}\frac{\partial}{\partial r}(rv_r) + \frac{1}{r}\frac{\partial v_\phi}{\partial \phi} + \frac{\partial v_z}{\partial z} = 0 , \tag{3a}$$

$$D'v_r - \frac{v_\phi^2}{r} - 2(1+\tau_z)v_\phi + 2\tau_\phi v_z = \tag{3b}$$

$$-\frac{\partial p_d}{\partial r} + \frac{1}{Re}\left[D''v_r - \frac{v_r}{r^2} - \frac{2}{r^2}\frac{\partial v_\phi}{\partial \phi}\right] ,$$

$$D'v_\phi + \frac{v_r v_\phi}{r} + 2(1+\tau_z)v_r - 2\tau_r v_z = \tag{3c}$$

$$-\frac{1}{r}\frac{\partial p_d}{\partial \phi} + \frac{1}{Re}\left[D''v_\phi - \frac{v_\phi}{r^2} + \frac{2}{r^2}\frac{\partial v_r}{\partial \phi}\right] ,$$

$$D'v_z + 2\tau_r v_\phi - 2\tau_\phi v_r = -\frac{\partial p_d}{\partial z} - 2r\tau_r + \frac{1}{Re}D''v_z , \tag{3d}$$

where

$$D' = \frac{\partial}{\partial t} + \frac{\partial}{\partial \phi} + v_r\frac{\partial}{\partial r} + \frac{v_\phi}{r}\frac{\partial}{\partial \phi} + v_z\frac{\partial}{\partial z} ,$$

$$D'' = \frac{\partial^2}{\partial r^2} + \frac{1}{r}\frac{\partial}{\partial r} + \frac{1}{r^2}\frac{\partial^2}{\partial \phi^2} + \frac{\partial^2}{\partial z^2} .$$

and

$$\tau_r = -\epsilon\cos\phi \ , \ \tau_\phi = \epsilon\sin\phi \ , \ \tau_z = \tau\cos\theta \ , \ \epsilon = \tau\sin\theta \ . \tag{4}$$

The primary effect of nutation is contained in the ϕ-periodic force term $-2r\tau_r = 2\epsilon r\cos\phi$ in the z-momentum equation (3d). If this term vanishes throughout, $\epsilon = 0$, equations (3) support a trivial solution $\mathbf{v}_d \equiv 0$, $p_d \equiv 0$.

The system (3) of equations is similar to the system numerically solved by Vaughn et al. (1983; 1985), but simplified by introducing the reduced pressure p_d. We also note that this system supports certain symmetries. Let v_r, v_ϕ, v_z and p_d be the solution at point r,ϕ,z, then the velocities and pressure at the corresponding point $r,\phi+\pi,-z$ are $v_r, v_\phi, -v_z$ and p_d. These symmetries can be exploited for essential savings in computational work.

2.1 *Linearized equations*

For sufficiently small $\epsilon \neq 0$, it is obvious that the deviation velocity is of order $O(\epsilon)$. In the situations of practical interest, $\epsilon = (\Omega/\omega)\sin\theta$ turns out to be a rather small parameter. Even a conservative estimate with $\Omega \leq 500$ rpm, $\omega \geq 3000$ rpm, and $\theta \leq 20°$ provides values of $\epsilon \leq 0.054$. Consequently, it seems well justified to linearize the equations in ϵ. This linearization imposes no restriction on the Reynolds number.

While the continuity equation remains unaffected, linearization of the momentum equations provides

$$D^* v_r - 2(1+\tau_z)v_\phi = -\frac{\partial p_d}{\partial r} + \frac{1}{Re}\left[D'' v_r - \frac{v_r}{r^2} - \frac{2}{r^2}\frac{\partial v_\phi}{\partial \phi}\right] , \tag{5a}$$

$$D^* v_\phi + 2(1+\tau_z)v_r = -\frac{1}{r}\frac{\partial p_d}{\partial \phi} + \frac{1}{Re}\left[D'' v_\phi - \frac{v_\phi}{r^2} + \frac{2}{r^2}\frac{\partial v_r}{\partial \phi}\right] , \tag{5b}$$

$$D^* v_z = -\frac{\partial p_d}{\partial z} - 2r\tau_r + \frac{1}{Re}D'' v_z \ . \tag{5c}$$

where

$$D^* = \frac{\partial}{\partial t} + \frac{\partial}{\partial \phi} .$$

The system (3a), (5a)-(5c) of equations is still quite difficult to solve. Any serious attempt to satisfy all boundary conditions leads directly to a purely computational approach. Use of the boundary-layer approximation would simplify the task but seems inappropriate in the interesting range of low Reynolds numbers.

3. The core flow

We recall that the flow in a relatively long cylinder (aspect ratio $\lambda = 4.3$) at low Reynolds number is expected to have a rather simple structure and to provide a roll moment proportional to Re (Herbert 1982). Closer analysis of the equations suggests that this flow exhibits little axial variation over much of the cylinder length. The effect of the end walls will be essential only over an axial distance of $O(1)$ from the ends. Therefore, we have relaxed the boundary conditions at the end walls. In this way, we seek a steady flow in a finite segment of an infinitely long cylinder.

The z-independent force term in eq. (5c) can be balanced only by a purely axial deviation velocity. It is consistent with the linearized equations to assume a solution in the form

$$\mathbf{v}_d = (0,0,v_z) \ , \quad p_d = 0 \ . \tag{6}$$

Moreover, since v_z is of order $O(\epsilon)$ and periodic in ϕ, we write

$$v_z = v_z(r,\phi) = 2\epsilon[f(r)\cos\phi + g(r)\sin\phi] \ , \tag{7}$$

where f and g are the imaginary and real parts, respectively, of the complex function

$$F(r) = g(r) + i f(r) \tag{8}$$

Substituting (6)-(8) into the linearized equations and the no-slip conditions at the cylinder wall provides

$$r^2F'' + r\,F' - (1 + i\,Re\,r^2)F = -\,i\,Re\,r^3 \ , \tag{9a}$$

$$F = 0 \ \text{ at } \ r = 1 \ , \tag{9b}$$

$$F \text{ finite at } \ r = 0 \ , \tag{9c}$$

where (9c) is necessary for a physical solution. The primes denote d/dr.

3.1 *Solution for* $Re \to 0$ and $Re \to \infty$

For $Re \to 0$, the solution of equations (9) equations can be found in the form of series expansions in Re,

$$f = \frac{Re}{8}(r - r^3) - \frac{Re^3}{9216}(7r - 12^3 + 6r^5 - r^7) + O(Re^5) , \tag{10a}$$

$$g = \frac{Re^2}{192}(2r - 3r^3 + r^5) + O(Re^4) . \tag{10b}$$

With higher terms included, these series converge for $Re \leq 12$.

In the limit $Re \to \infty$, one obtains

$$f \to 0, \quad g \to r \quad \text{as} \quad Re \to \infty. \tag{11}$$

Owing to the loss of the highest derivatives, however, this solution cannot satisfy the boundary conditions (9b) and is valid only outside thin boundary layers near the wall at $r = 1$.

Even without any knowledge of the solution in the intermediate range, the different character of the basic flow at low and high Reynolds numbers is evident. At low Re, the component f in the x,z-plane $\phi = 0$ dominates the solution. At high Re, f is negligible except near the wall of the cylinder while g in the y,z-plane $\phi = 90^o$ is dominating. One might well expect that the initial linear increase of f with Re and the change in the flow structure is related to the observed properties of the roll moment.

3.2 *Solution for arbitrary values of Re*

In earlier work (Herbert 1983), we have applied a spectral collocation method for numerically solving a real system of equations for f and g equivalent to eqs. (9). Series in odd Chebyshev polynomials for the interval $0 \leq r \leq 1$ provide accurate solutions at rather low truncation. This experience together with the minor effect of harmonics in the azimuthal direction at small ϵ suggests the use of spectral methods for efficiently solving the nonlinear equations (3).

Here, we derive an analytical solution for the core flow in a sufficiently long cylinder. A particular solution of the inhomogeneous equation (9a) is $F_0 = r$, whereas the homogeneous part of (9a) is the equation for the modified Bessel functions $I_1(qr)$ and $K_1(qr)$ of the complex argument qr where $q = (1 + i)(Re/2)^{1/2}$. In order to satisfy (9c), $K_1(qr)$ cannot contribute to the solution. Finally, (9b) provides

$$F(r) = g + i f = r - I_1(qr)/I_1(q) \ . \tag{12}$$

This solution is valid for arbitrary Re but may be unstable as Re exceeds some critical value. Although expressible in simple form, the resulting flow field exhibits very interesting properties.

Rewriting the solution in terms of Kelvin functions of real argument is of little advantage for the numerical evaluation. We have used a combination of ascending series and asymptotic expansions for large arguments (Abramowitz & Stegun 1972) for evaluating $F(r)$. With the solution (12) at hand, it is straightforward to derive the approximations (10) from the ascending series for I_1 (and to explain the convergence problem for larger Re). Complementary to (11), the asymptotic expansion for large arguments, i.e. large Reynolds numbers provides the boundary-layer behavior

$$F \approx r - \sqrt{r}\ e^{q(r-1)} \ . \tag{13}$$

This expression agrees to within 1% with (11) provided $r \leq 1-\delta$. The boundary layer thickness δ can be obtained from the transcendental equation

$$\delta = \sqrt{2/Re}\ [4.605 - \frac{3}{2}\ln(1 - \delta)] \ , \tag{14}$$

e.g., $\delta = 0.223$ for $Re = 1000$.

3.3 *The velocity field*

We have chosen three different graphical representations in order to illustrate the characteristic changes of the velocity distribution over the cylindrical cross section with increasing Re. Figure 2 shows the components f (in the x,z-plane) and g (in the y,z-plane) for a wide range of Reynolds numbers. The opposite sign of the velocity at diametral points assures zero net flux of mass through the cross section. The curves represent cuts through the contour plots of these functions of r and Re in figure 3 at the tick marks $Re = 1, 10, 100,$ and 1000. Up to $Re \approx 5$, the velocity distribution is governed by f. This component never exceeds a value of 0.4, assumes a maximum at $Re \approx 20$ and retains significant size only in a shrinking

neighborhood of the wall as Re increases. The component g rapidly increases from negligible values as $Re > 5$ and approaches the linear increase with r according to (11) except near the wall at $r = 1$. In figure 4, the data of figure 2 are combined into contour plots of the axial velocity $v_z/(2\epsilon)$ over the cylindrical cross section. These plots clearly show the shift of the velocity maximum (marked by +) from $\phi \approx 0$ at $Re = 1$ to $\phi \approx 90°$ at $Re = 1000$. Figure 4d also illustrates the ramp-like velocity distribution over most of the cross section and the boundary layers with $\delta = 0.223$.

Superposition of the deviation velocity $\mathbf{V}_d$ and the solid body rotation $\mathbf{V}_s$ according to eq. (2) leads to an azimuthally periodic velocity field $\mathbf{V}_n$ which is steady in the nutating frame. The paths of fluid elements are circular orbits about axes that are inclined to the z-axis. The inclination depends on radius and Reynolds number.

Figure 5 compares the dimensional velocity distributions obtained from (7), (12) with computational results for the center cross-section ($z = 0$) of a cylinder of aspect ratio 4.3.* The agreement for $Re = 14.9$ is considered representative for the range of lower Reynolds numbers. We have repeated the numerical simulation of the flow at this Reynolds number with a modified version of the Sandia code and obtained very small components $|v_r| < 0.005$ m/s, $|v_\phi| < 0.05$ m/s at $z = 0$. These results verify our estimates and justify the use of linearized equations. Moreover, disregarding the presence of end walls seems to have little effect in the center portion of the cylinder. The radial distribution of V_z in the range $-3.5 \leq z \leq 3.5$ is nearly identical with the data shown in figure 5.

Figure 6 shows a similar comparison for $Re = 45.7$. At this higher Reynolds number, we find a systematic deviation between the theoretical result and numerical results at different axial positions. We attribute this deviation to a superposed cellular motion that is not yet incorporated into our analysis.

* The data were kindly provided by H. R. Vaughn, Sandia National Laboratories.

4. Moments

Considered that a solid payload, or a liquid payload in pure solid-body motion, would allow for a stable flight of a projectile, we can fully concentrate on the moments caused by the deviation velocity $\mathbf{V}_d$. With $\mathbf{V}_d = (0, 0, \omega a v_z)$ and v_z given, the moments on a finite-length section of the cylinder can be calculated. We consider a control volume R (surface S) formed by the solid cylindrical wall and liquid surfaces at both ends. The choice of a solid wall as the cylindrical boundary is important for capturing the roll moment. Conservation of angular momentum requires

$$\mathbf{M} = \frac{\partial}{\partial t} \int\int_R \int (\mathbf{r} \times \mathbf{V}_d) \rho \, dR + \int\int_R \int [\mathbf{r} \times (2\boldsymbol{\Omega} \times \mathbf{V}_d)] \rho \, dR \tag{15}$$

$$+ \int\int_S \int (\mathbf{r} \times \mathbf{V}_d)(\mathbf{V}_d \cdot \mathbf{n}) \rho \, dS + \int\int_S \int (\mathbf{r} \times \mathbf{V}_s)(\mathbf{V}_d \cdot \mathbf{n}) \rho \, dS \ ,$$

where $\mathbf{n}$ is the outer unit normal. On the left-hand side, $\mathbf{M}$ is the resultant torque on the control volume. Note that the shear moment vanishes at the solid side wall while the contributions from the liquid end surfaces cancel. On the right-hand side, the first term vanishes for steady $\mathbf{V}_d$. The second term originates from Coriolis forces in the nutating system. The third term vanishes since $\mathbf{V}_d$ has only an axial component. The last term provides the net rate of angular momentum flux through the control surface.

Substitution of $\mathbf{V}_d$ leads to the following expressions for the cartesian components of $\mathbf{M}$:

$$M_x = m_l (2\Omega \, a \sin\theta)(\omega a) \; m_x \ , \ m_x = -\int_0^1 r^2 f \, dr \ , \tag{16a}$$

$$M_y = m_l (2\Omega \, a \sin\theta)(\omega a) \; m_y \ , \ m_y = -\int_0^1 r^2 g \, dr \ , \tag{16b}$$

$$M_z = m_l (2\Omega \, a \sin\theta)^2 \, m_z \ , \ m_z = \int_0^1 r^2 f \, dr = -\, m_x \ , \tag{16c}$$

where $m_l = 2\pi \rho a^2 c$ is the liquid mass in the cylinder. In this form, the components M_x, M_y represent the net rate of angular momentum flux through the liquid ends, whereas the roll moment M_z is solely due to Coriolis forces. A close relation between roll moment M_z and yaw

moment M_z has also been found by Murphy (1984, 1985). Note that M_x, M_y after division by $m_c\omega^2 a^2$ clearly are of order $O(\epsilon)$. M_z however is of order $O(\epsilon^2)$, and the question arises whether (16c) will be affected by second-order terms. Analysis of higher-order approximations† indicates, however, that (16c) is correct to within $O(\epsilon^2)$.

A different physical interpretation of the moments can be derived using the differential equation (9a), integrating by parts, applying (9b), and separating real and imaginary parts:

$$m_z = -m_z = \int_0^1 r^2 f dr = -\frac{g'(1)}{Re}\,, \tag{17a}$$

$$m_y = -\int_0^1 r^2 g dr = -\frac{f'(1)}{Re} - \frac{1}{4}\,. \tag{17b}$$

In this form, the moments are directly related to the shear forces at the cylindrical sidewall, $r = 1$. Since $f'(1) < 0$, $g'(1) < 0$, the roll moment M_z is always positive (even for $\Omega < 0$), while M_x is negative for $\Omega > 0$ and changes sign with Ω. For small Re, the series (10) provide the approximations

$$m_z \approx \frac{Re}{96}\,,\ m_y \approx -\frac{Re^2}{1536}\,, \tag{18}$$

that can be used for quick estimates up to $Re \leq 10$. The linear increase of m_z and M_z with Re is consistent with the experimental data. From the analytical solution (10), we obtain

$$F'(1) = g'(1) + i f'(1) = 2 - qI_0(q)/I_1(q). \tag{19}$$

Substitution into (17) provides the variation of m_z, m_y with the Reynolds number shown in figure 7. The coefficient m_z assumes a pronounced maximum at $Re \approx 19$. The occurrence of this maximum was earlier thought to originate from hydrodynamic instability with respect to a cellular motion. Here, we find a simple explanation in the properties of the axial velocity component f in the $x,z-$plane and the derivative $g'(1)$. The coefficient m_y is negligible for

†Detailed results for higher-order approximations will be published elsewhere.

$Re < 5$, sharply decreases with increasing Re and reaches an asymptotic value of $m_y \to -1/4$ as $Re \to \infty$. Hence, for $\Omega > 0$, M_y tends to reduce the pitch moment due to the solid body rotation. We note, however, that these moments represent only the effect of viscous shear at the cylindrical side wall. Shear at the end walls and the contribution of the pressure are neglected.

The data base for the yaw and pitch moments is scarce. Computations by Vaughn et al. (1985) indicate, however, that the pressure contributions to these moments are larger (and opposite in sign) than the viscous components. Only the viscous component can be estimated from our solution. Therefore, we concentrate in the following on a detailed comparison for the roll moment.

In figure 8 we compare the asymptotic law (18) and the theoretical result (17) with experimental data (Miller 1982) and computational results (Vaughn et al. 1985) for the roll coefficient m_z on a doubly logarithmic scale. The initial spin rate $\omega = 4000$ rpm has been used for obtaining the nondimensional values from the experiment. For $Re < 10$, the experimental data match the analytical result as well as the asymptotic law $m_z \approx Re/96$. The deviation between theoretical and computational results is probably due to a larger axial extent of the end effects at very low Reynolds numbers. Good agreement with the computational results is obtained near the maximum of m_z. The point at $Re = 113$ is close to the Reynolds number where the numerical simulation fails to converge to a steady solution, and may not be very accurate. The experiments find the maximum roll moment at slightly lower Reynolds numbers than the theoretical value. In fact, this discrepancy will increase as lower spin rates ω are used for data reduction. In view of the agreement between theoretical and computational results, the discrepancy can not arise from the approximations employed in our analysis. A first possible source may be the effect of unsteadiness in the spin-down experiments. More likely, however, the shift is caused by changes of temperature and viscosity during the experiments. A moderate increase in temperature would reduce the viscosity of the working fluids (silicone oil, corn syrup) and hence shift the maximum to higher Reynolds numbers. Miller (personal communication) observed a temperature increase by $\approx 2.5°C$ per run up to $\approx 10°C$ above ambient temperature after repeated runs. Vaughn et al. (1985) used these values for correcting the results, with some improved agreement. We waive such a correction but discuss the temperature increase in more detail in the next chapter.

As a final observation in figure 8, we note the change in tendency for the two experimental data points at $Re > 10^3$. It is likely that the internal flow becomes unsteady and ultimately turbulent as the Reynolds number increases. Preliminary results from flow visualization in a small-scale experiment (Pierpont 1985) indicate that these two points are for a turbulent internal flow.

In figure 9 we recast experimental, computational and theoretical results for the dimensional roll moment M_z in different form. Whereas the asymptotic properties are concealed, the linear scale for M_z reveals the pronounced maximum of the roll moment for viscosities near $\nu = 10^5$ cSt and more clearly indicates that theory and computation yield larger maximum values than the despin experiments with the old test fixture (Miller 1982). More recent measurements with a new test fixture at higher spin rates (Miller, personal communication) provide larger maximum values slightly in excess of the theoretical result.

For the roll moment as a function of nutation angle and rate, Herbert (1983) derived from Miller's data (1982, fig. 12) the empirical relation $M_z = 0.00814\,(\Omega \sin\theta)^2$ Nm. The theory provides M_z in the same form but with a somewhat larger factor of 0.0111. This comparison for a fluid of kinematic viscosity $\nu = 2{\cdot}10^5$ cSt is likely to be biased by temperature effects. A notable feature of the roll moment as a function of nutation rate at different spin rates is shown in figure 10. For these parameters in the range of the maximum roll moment, the dependence of M_z on ω is non-monotonic, e.g. the data for $\omega = 9000$ rpm are in between those for $\omega = 3000$ and 6000 rpm. This puzzling behavior has been observed by Miller in experiments with the new test fixture. From the theoretical result it is obvious that M_z decreases (increases) with ω for sufficiently small (large) viscosities to the left (right) of the maximum in figure 9.

The interpretation of the experimental results has been hampered by the observation of Miller (1982) that "the despin moment was not a function of the canister spin rate, provided a sufficient spin rate is present". In contrast, the theoretical result (14c),(15a),(19) depends on the spin rate since $q \sim Re^{1/2}$ and $Re \sim \omega$ for fixed a and ν. Figure 11 shows the theoretical results for M_z as a function of the spin rate ω for viscosities $\nu = 10^3$, 10^4, and 10^5 cSt on linear scales. Note that in some range of ω, M_z appears indeed nearly independent of the spin rate, especially for $\nu = 10^5$ cSt where the maximum of M_z stretches out over most of the observed range ($3000 < \omega < 9000$ rpm) of spin rates. Figure 11 also shows different prototypes of behavior that are distinguished by the position of the maximum roll moment along the ω axis.

Experimental data for similar conditions are shown in figure 12 and verify the theoretically predicted behavior. Moreover, these data suggest major simplifications in the experimental procedures. Whereas the experimental data in figure 9 were obtained by using numerous working fluids of different viscosities, a more complete set of data can be generated by carefully monitoring the spin-down for a few runs with fluids in the range of low, medium, and high viscosities as in figure 12.

5. Temperature effect

The comparison of theoretical and computational results with experimental data seems to be biased by the effect of increasing temperature on the viscosity of the working fluid. These effects appear more pronounced at high viscosities and high spin rates. For an estimate of the rate of change of the average temperature T, we consider a control volume R (surface S) formed by liquid surfaces along the cylinder's side and end walls. The material properties are assumed to be constant and heat transfer through the surface is disregarded. Balancing the rate of change of energy with the work done on the control volume, we obtain after some simplifications

$$m_l\, c_v \frac{dT}{dt} = \int_S \int \boldsymbol{\tau} \cdot \mathbf{V}_i \, dS, \tag{20}$$

where c_v is the specific heat, τ the vector of tangential stresses, and $\mathbf{V}_i$ the velocity measured in an inertial frame. Since $\mathbf{V}_d$ is independent of z, the contributions from the cylinder ends cancel. The only contribution is due to the shear stress

$$\tau_{rz} = \mu \frac{\partial(\omega a v_z)}{\partial r}\Big|_{r=1} = 2\mu\Omega\, a \sin\theta \,[f'(1)\cos\phi + g'(1)\sin\phi] \quad . \tag{21}$$

in the axial direction. The relevant axial component of the velocity $(\boldsymbol{\Omega} + \boldsymbol{\omega}) \times \mathbf{r}$ of some point on the surface S is given by $-\Omega\, a \sin\theta \sin\phi$. Integration over the cylindrical surface yields

$$m_l\, c_v \frac{dT}{dt} = -\mu (2\Omega\, a \sin\theta)^2 \pi\, a c\, g'(1) \; . \tag{22}$$

After substituting for m_l and introducing the Reynolds number, this result can be written as

$$\frac{dT}{dt} = \frac{\omega}{2c_v} (2\Omega\, a \sin\theta)^2 \left(-\frac{g'(1)}{Re}\right) \; . \tag{23}$$

Comparison with eq. (15a) shows that the rate of change of temperature can be directly expressed in terms of the roll moment,

$$\frac{dT}{dt} = \frac{\omega}{2c_v} (2\Omega\, a \sin\theta)^2\, m_z = \frac{\omega}{2 m_l\, c_v} M_z \; . \tag{24}$$

This result immediately shows that the temperature rise per run cannot be specified as a single number, nor should a uniform correction be applied to the experimental data. Moreover, the temperature changes increase with the spin rate, and consequently are quite different for the experiments with the old (Miller 1982) and the new test fixture. Using the maximum value $m_z \approx 0.0854$, we obtain for the 1982 experiments ($a = 60.3$ mm, $\omega = 4000$ rpm, $\Omega = 500$

rpm, $\theta = 20°$) with corn syrup ($c_v \approx 2350$ J/kg°C)) a temperature rise of $dT/dt = 0.036$°C/s. Using silicone oil ($c_v \approx 1600$ J/kg°C)) in the new test fixture ($a = 55.4$ mm, $\omega = 10^4$ rpm, $\Omega = 600$ rpm, $\theta = 20°$) leads to a temperature increase of $dT/dt = 0.158$°C/s.

A single run consists of three phases (Miller, personal communication). The spin-up period of ≈ 30 s is followed by a sudden start of the nutational motion and a period of ≈ 30 s in order to reach steady conditions. Finally, the shutdown of the spin drive is followed by a spin-down period of ≈ 15 s. The second period at nearly steady conditions and maximum spin rate appears most relevant to the modification of the viscosity. During this period, the kinematic viscosity of corn syrup changes according to $\nu = \nu_0 e^{-0.119\Delta T}$, where ν_0 is the nominal kinematic viscosity at the beginning of the run. At the start of the third phase, the average temperature may have increased by $\Delta T \approx 1.07$°C, while the viscosity dropped to $\nu \approx 0.88\nu_0$. Measurements by Miller indicated that the temperature in the cylinder after repeated runs stabilized at $\Delta T \approx 10$°C above ambient temperature. At this level, the viscosity would be reduced to $\nu \approx 0.3\nu_o$. This effect would fully account for the systematic deviation between experimental and theoretical data in figure 9. In the more recent experiments at higher spin and nutation rates, the average temperature may have increased by as much as $\Delta T \approx 4.75$°C over a period of 30 seconds. The value of 2.5°C measured in the new fixture is well within the estimated range. The temperature effect on the kinematic viscosity of silicone oils, however, is relatively small. With $\nu = \nu_0 e^{-0.014\Delta T}$, we obtain after 30 seconds $\nu \approx 0.94\nu_0$, and $\nu \approx 0.87\nu_0$ with $\Delta T = 10$°C after repeated runs.

6. Concluding remarks

We have developed a simple model of the viscous fluid motion in a spinning and nutating cylinder. The disregard of the end walls has some obvious consequences: the turning flow near the ends and the associated contributions of pressure and shear stresses to the moments cannot be obtained from this model. Nevertheless, we gather understanding as well as quantitative information. The velocity field of the core flow agrees well with computational results for low Reynolds numbers. The analytical result is an evident example for the formation of boundary layers. The core flow can be utilized as a basic flow in studies of hydrodynamic instability with respect to cellular motions. The parametric excitation of such cells by the azimuthally periodic deviation has been discussed by Herbert (1984). The core flow also represents the lowest-order approximation to the solution of the nonlinear equations (3) and can be extended by higher-order terms in ϵ.

The roll moment agrees well with measured and computed values, and can also be found at Reynolds numbers too large for successful numerical simulations. The roll moment originates from Coriolis forces. While the direct calculation of the yaw moment suffers from neglecting the pressure contribution, the yaw moment can be found from the roll moment using the relations given by Murphy (1984, 1985). The pitch moment remains an open issue. The estimates for the change in average temperature need further verification once more detailed data become available.

The simple form and scaling relations of our results provide guidance for sorting and evaluating the experimental data base. The results also suggest various improvements in the experimental procedures. First, the changes in temperature and viscosity should be carefully monitored. With the effective viscosity known, a closer agreement between theory and observation is to be expected. Second, the yet neglected variation of the roll moment with the spin rate is considered relevant and in fact provides the roll moment in some range of Reynolds numbers. Instead of producing the data for figure 9 by using numerous viscosities at fixed spin rate, very similar data can be generated by varying the spin rate for a few fluids.

ACKNOWLEDGMENT

The open cooperation and sharing of data with Miles C. Miller (CRDC) and Harold R. Vaughn (Sandia Laboratories) are greatly appreciated. Ri-Hua Li deserves credit for his assistance in developing the analytical solution. This work is supported by the Army Research Office under Contract DAAG29-82-K-0129 and by the Army AMCCOM under Contract DAAK11-83-K-0011.

REFERENCES

Abramowitz, M. & Stegun, I. A. 1972 " Handbook of Mathematical Functions," New York: Dover Publications, Inc.

D'Amico, W. P. 1977 "Field Tests of the XM761: First Diagnostic Test," Ballistic Research Laboratory, Memorandum Report 1325.

D'Amico, W. P. 1978 "Field Tests of the XM761: Second Diagnostic Test," Ballistic Research Laboratory, Memorandum Report ARBRL-MR-02806.

D'Amico, W. P. & Miller, M. C. 1979 "Flight Instability Produced by a Rapidly Spinning, Highly Viscous Liquid," *J. of Spacecraft and Rockets*, Vol. 16, pp. 62-64.

Herbert, Th. 1982 "Fluid Motion in a Rotating and Nutating Cylinder - Part I," Report prepared under the Scientific Services Program. Published as Report CRDC-CR-84087 (1984).

Herbert, Th. 1983 "The Flow of Highly Viscous Fluid in a Spinning and Nutating Cylinder," Proc. of the 1983 Scientific Conference on Chemical Defense Research, Aberdeen Proving Ground, MD.

Herbert, Th. 1984 "Highly Viscous Fluid Flow in a Spinning and Nutating Cylinder," Proc. of the Second Army Conference on Applied Mathematics and Computing, Troy, NY.

Miller, M. C. 1981 "Void Characteristics of a Liquid Filled Cylinder Undergoing Spinning and Coning Motion," *J. of Spacecraft and Rockets*, Vol. 18, pp. 286-288.

Miller, M. C. 1982 "Flight Instabilities of Spinning Projectiles Having Nonrigid Payloads," *J. of Guidance, Control, and Dynamics*, Vol. 5, pp. 151-157.

Murphy, C. M. 1984 "A Relationship between Liquid Roll Moment and Liquid Side Moment," Ballistic Research Laboratory Memorandum Report ARBRL-MR-03347.

Murphy, C. M. 1985 "A Relation between Liquid Roll Moment and Liquid Side Moment," *J. of Guidance, Control, and Dynamics*, Vol. 8, pp. 287-288.

Pierpont, D. 1985 "Design of an Experiment for Visualization of the Flow in a Spinning and Nutating Cylinder," Senior Project Report, VPI & SU.

Stewartson, K. 1959 "On the Stability of a Spinning Top Containing Liquid," *J. of Fluid Mech.*, Vol. 5, Part 4, pp. 577-592.

Vaughn, H. R., Oberkampf, W. L. & Wolfe, W. P. 1983 "Numerical Solution for a Spinning Nutating Fluid-Filled Cylinder," Sandia Report SAND 83-1789.

Vaughn, H. R., Oberkampf, W. L. & Wolfe, W. P. 1985 "Fluid Motion Inside a Spinning Nutating Cylinder," *J. of Fluid Mech.*, Vol. 150, pp. 121-138.

Wedemeyer, E. H. 1966 "Viscous Corrections to Stewartson's Stability Criterion," Ballistic Research Laboratory, Report 1325.

FIGURE CAPTIONS

Figure 1. Definition sketch

Figure 2. Components f and g of the axial velocity $v_z/(2\epsilon)$ for various Reynolds numbers: □, $Re = 1$; ○, 10; Δ, 10^2; +, 10^3.

Figure 3. Contour lines of the components f and g of the axial velocity $v_z/(2\epsilon)$ as a function of radius r and Reynolds number Re. Intervals are 0.05; the zero level is given by the heavy line.

Figure 4. Contour lines of equal axial velocity, $v_z/(2\epsilon) = \text{const.}$, for (a) $Re = 1$; (b) 10; (c) 10^2; (d) 10^3. Intervals are 0.01, 0.1, 0.2, 0.2, respectively. The zero level is given by the heavy line, the velocity maximum is marked by +.

Figure 5. Radial distribution of the dimensional velocity V_z at $z = 0$ for $Re = 14.9$. The symbols show the numerical solution to the Navier-Stokes equations (Vaughn 1983, personal communication). Parameters: $a = 60.3$ mm, $c/a = 4.3$, $\theta = 20^0$, $\omega = 3000$ rpm, $\Omega = 500$ rpm, $\rho = 1400$ kg/m^3.

Figure 6. Radial distribution of the dimensional velocity V_z at $z = 0$ for $Re = 45.7$. The symbols show the numerical solution to the Navier-Stokes equations (Vaughn 1983, personal communication). Parameters: $a = 60.3$ mm, $c/a = 4.3$, $\theta = 20^0$, $\omega = 3000$ rpm, $\Omega = 500$ rpm, $\rho = 1400$ kg/m^3.

Figure 7. The nondimensional coefficients m_z, m_y in eq. (17) vs. the Reynolds number Re.

Figure 8. Comparison of the theoretical result for m_z with: ×, experimental data (Miller 1982); ○, computational results (Vaughn et al. 1985). The straight line shows the asymptotic law $m_z \approx Re/96$.

Figure 9. Comparison of the theoretical result for the roll moment M_z at $\omega = 3000$ rpm vs. kinematic viscosity ν with: $\times$, experimental data (Miller 1982) for $\omega = 2000 - 4000$ rpm; $\bigcirc$, computational results (Vaughn et al. 1985) for $\omega = 3000$ rpm. Parameters: $a = 60.3$ mm, $c/a = 4.29$, $\theta = 20^0$, $\Omega = 500$ rpm. $\rho = 1000$ kg/m^3.

Figure 10. Theoretical results for the roll moment M_z vs. nutation rate Ω for different spin rates: Δ, $\omega = 3000$; $\bigcirc$, 6000; $\square$, 9000 rpm. Parameters: $a = 50.4$ mm, $c/a = 4.5$, $\theta = 20^0$, $\nu = 10^5$ cSt, $\rho = 1000$ kg/m^3.

Figure 11. Theoretical results for the roll moment M_z vs. spin rate ω for different kinematic viscosities: $\square$, $\nu = 10^3$; $\bigcirc$, 10^4, Δ, 10^5 cSt. Parameters: $a = 50.4$ mm, $c/a = 4.5$, $\theta = 20^0$, $\Omega = 625$ rpm, $\rho = 1400$ kg/m^3.

Figure 12. Experimental results for the roll moment M_z vs. spin rate ω for different kinematic viscosities: $\square$, $\nu = 10^3$; $\bigcirc$, 10^4, Δ, 10^5 cSt. Parameters: $a = 50.4$ mm, $c/a = 4.5$, $\theta = 20^0$, $\Omega \approx 600$ rpm, $\rho = 1400$ kg/m^3.

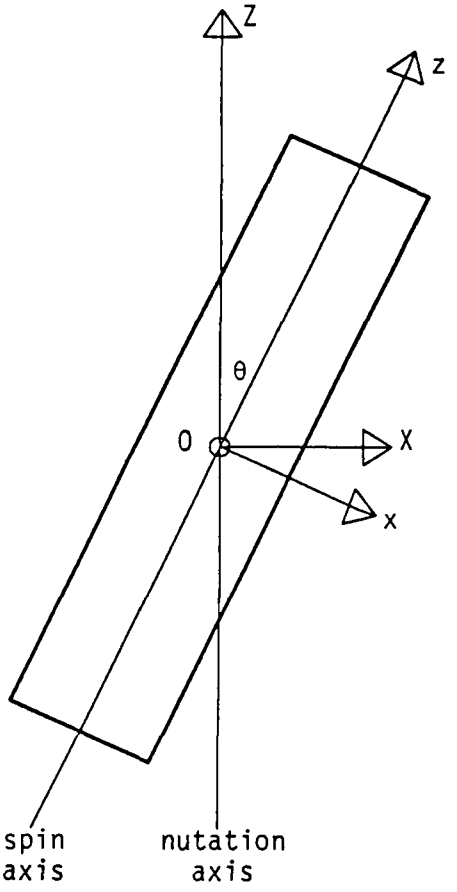

Figure 1.

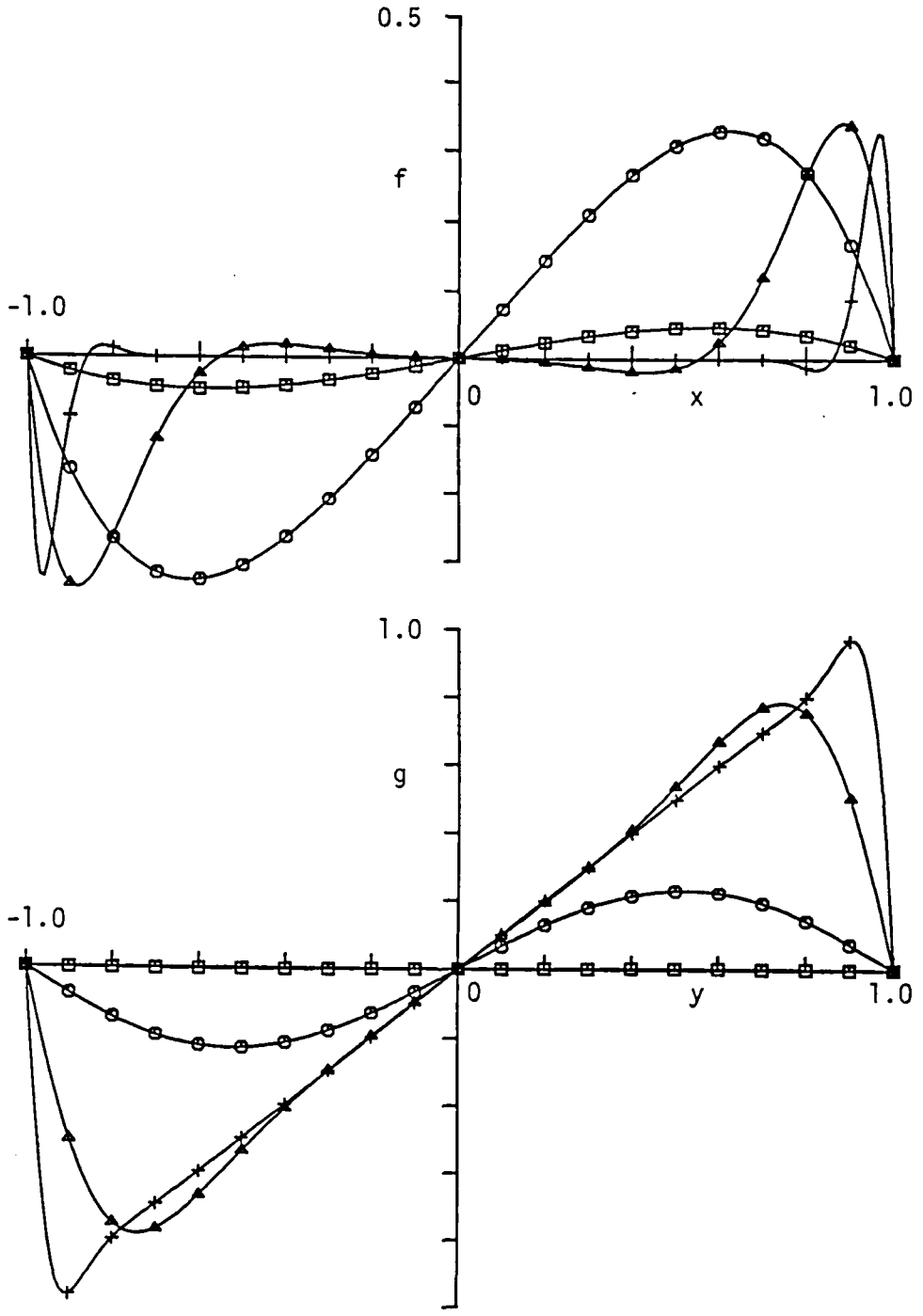

Figure 2.

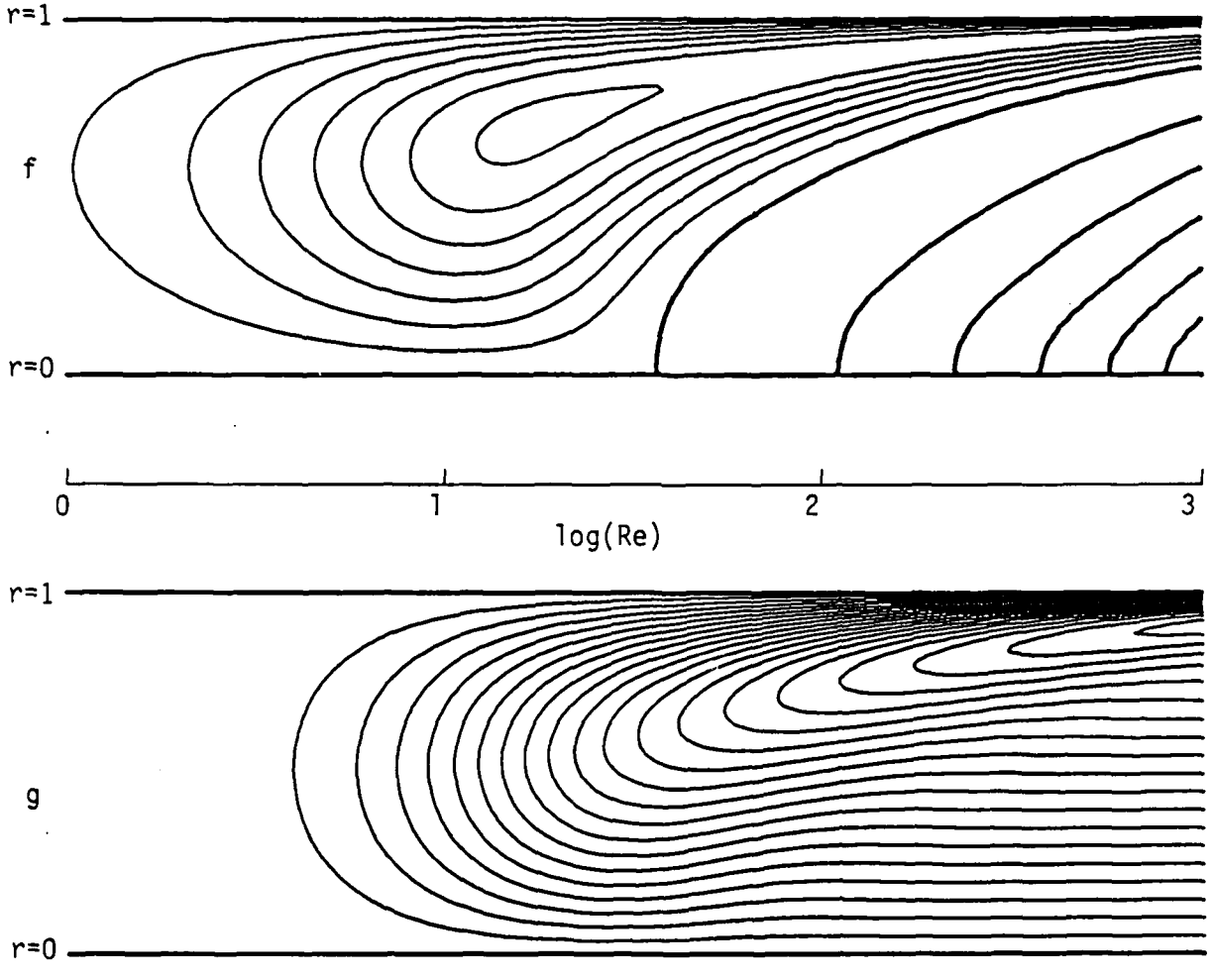

Figure 3

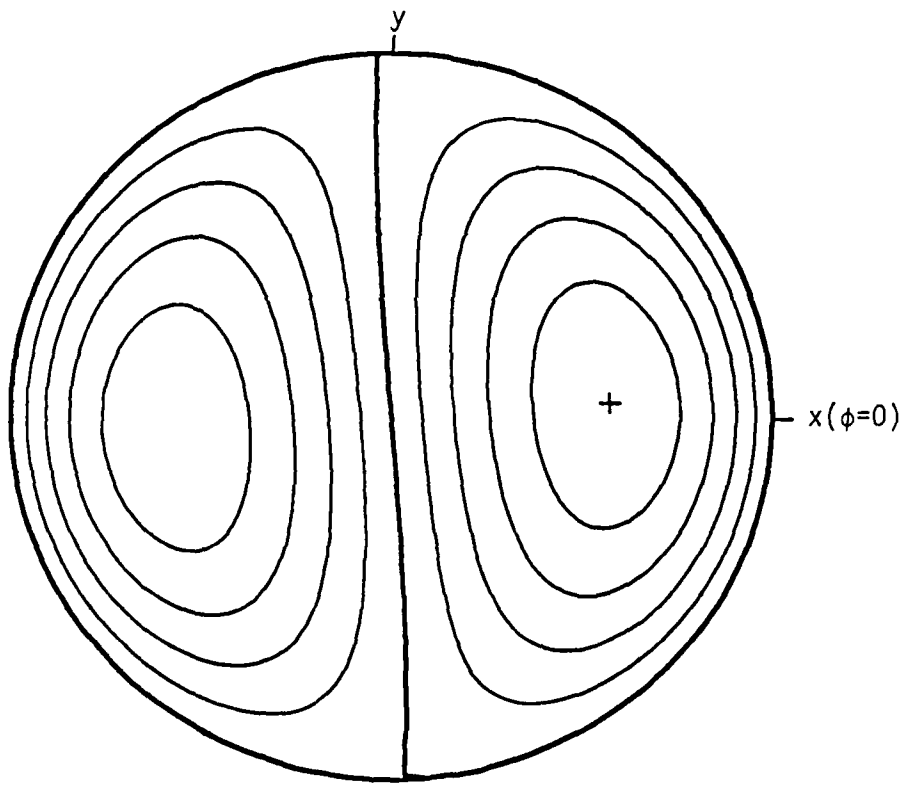

Figure 4a

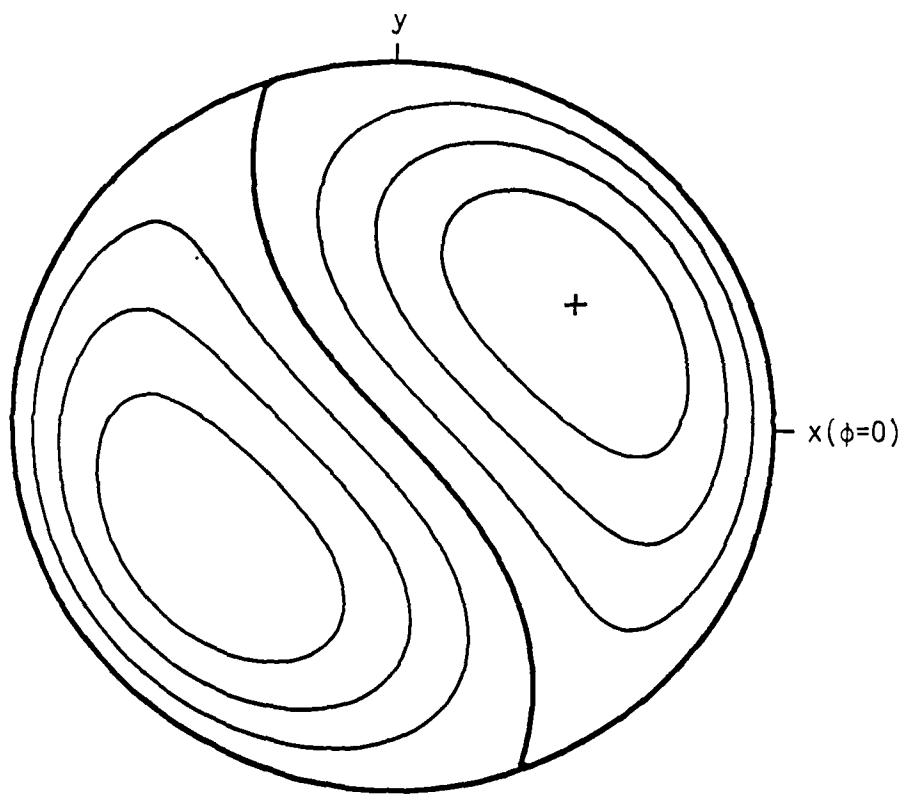

Figure 4b

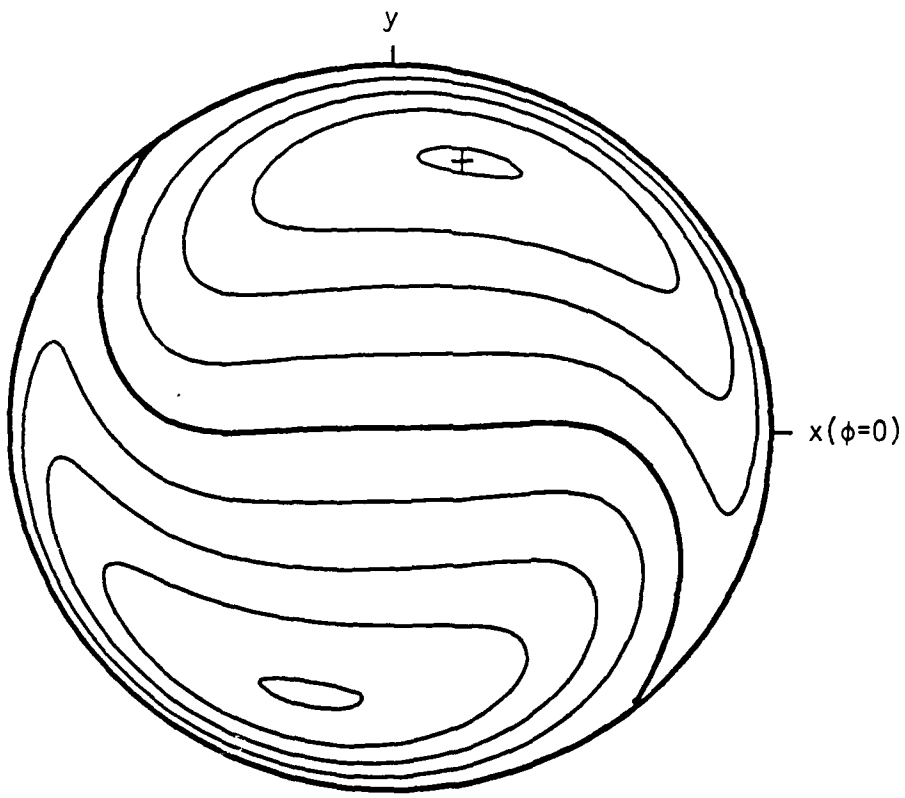

Figure 4c

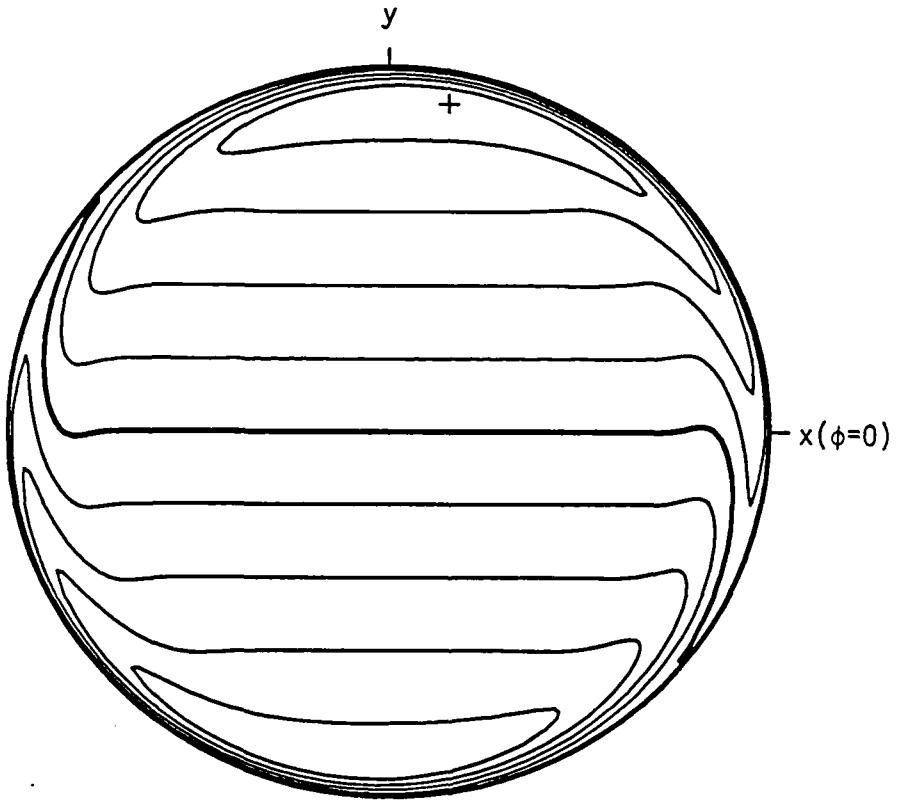

Figure 4d

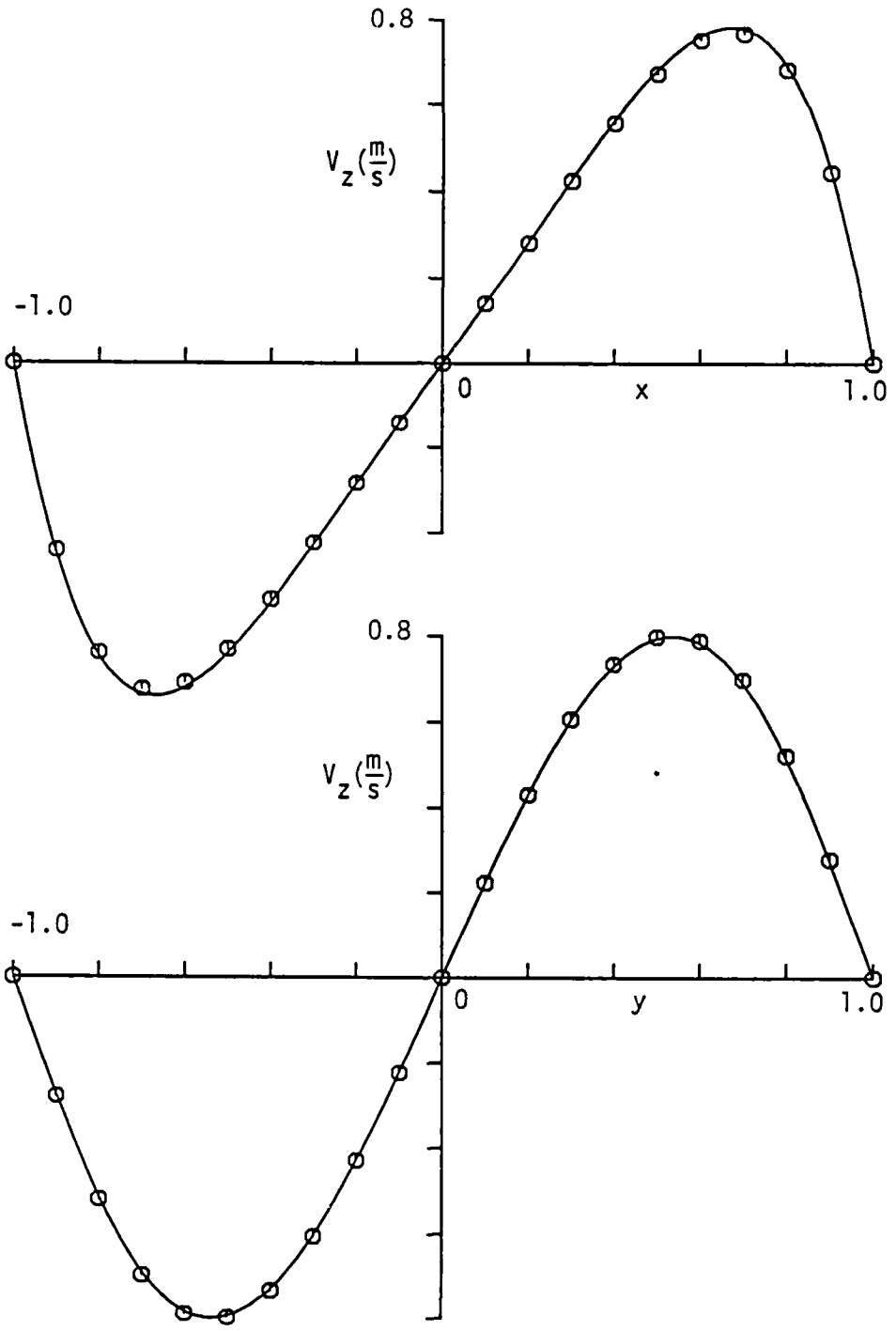

Figure 5

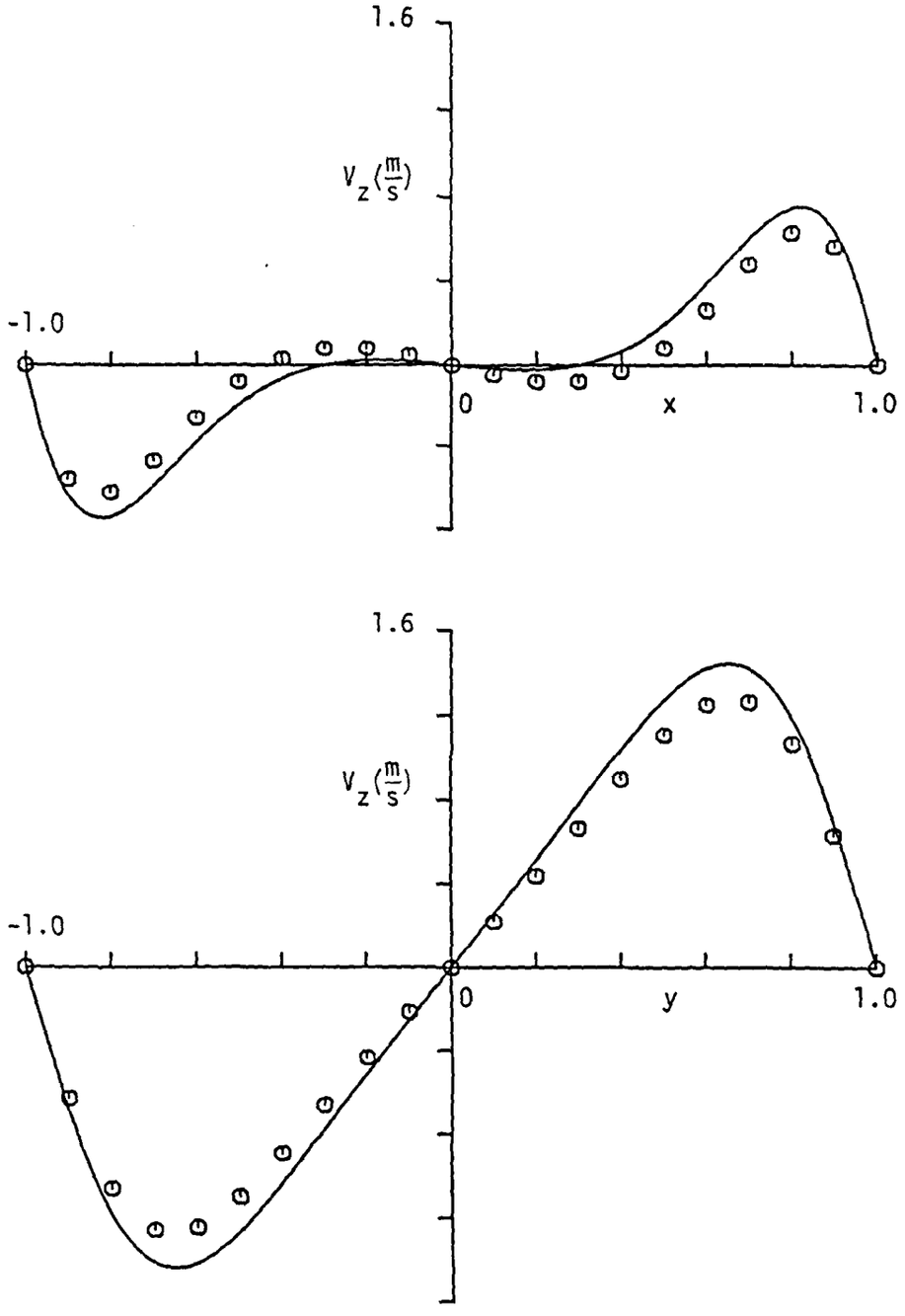

Figure 6

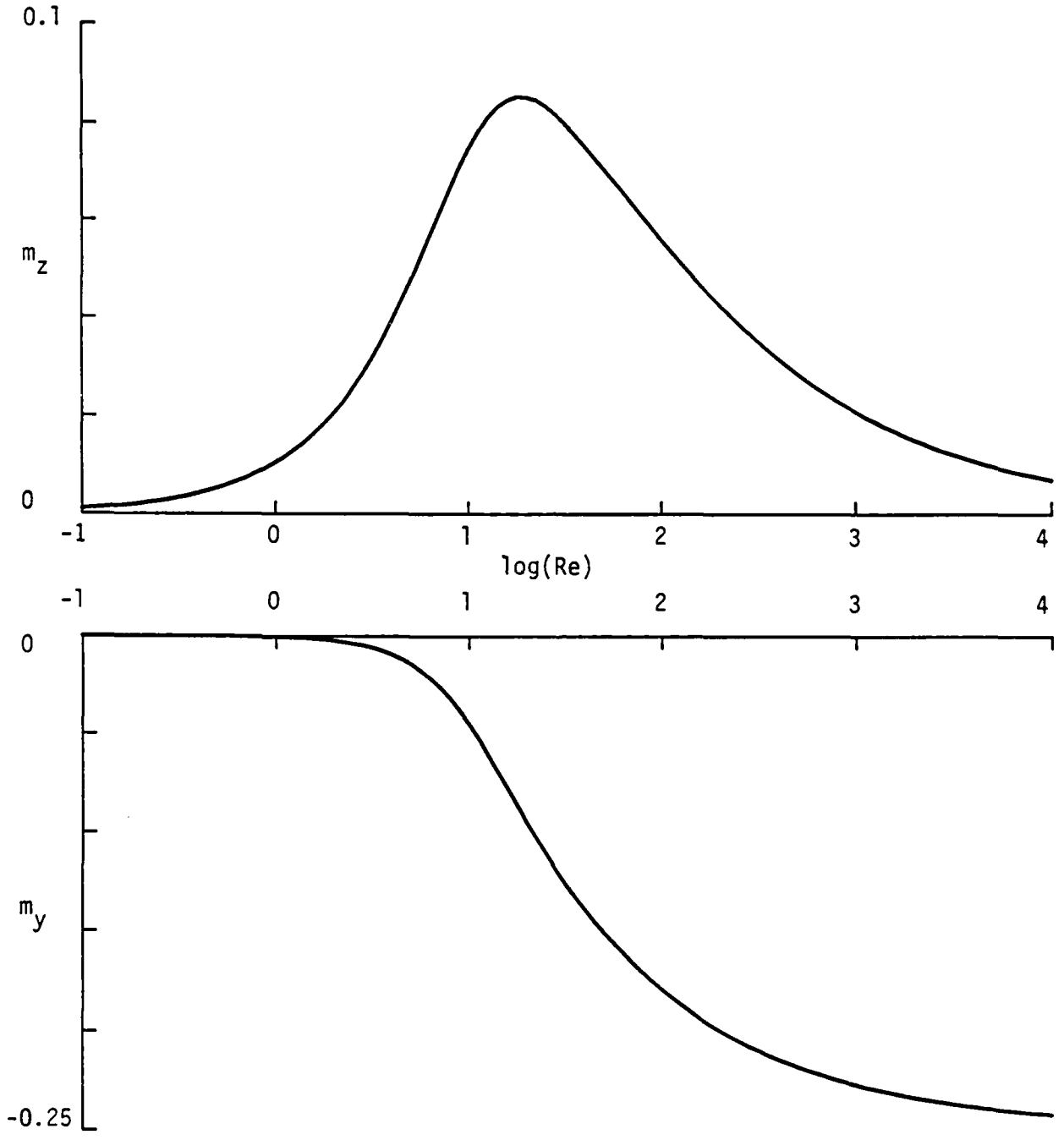

Figure 7

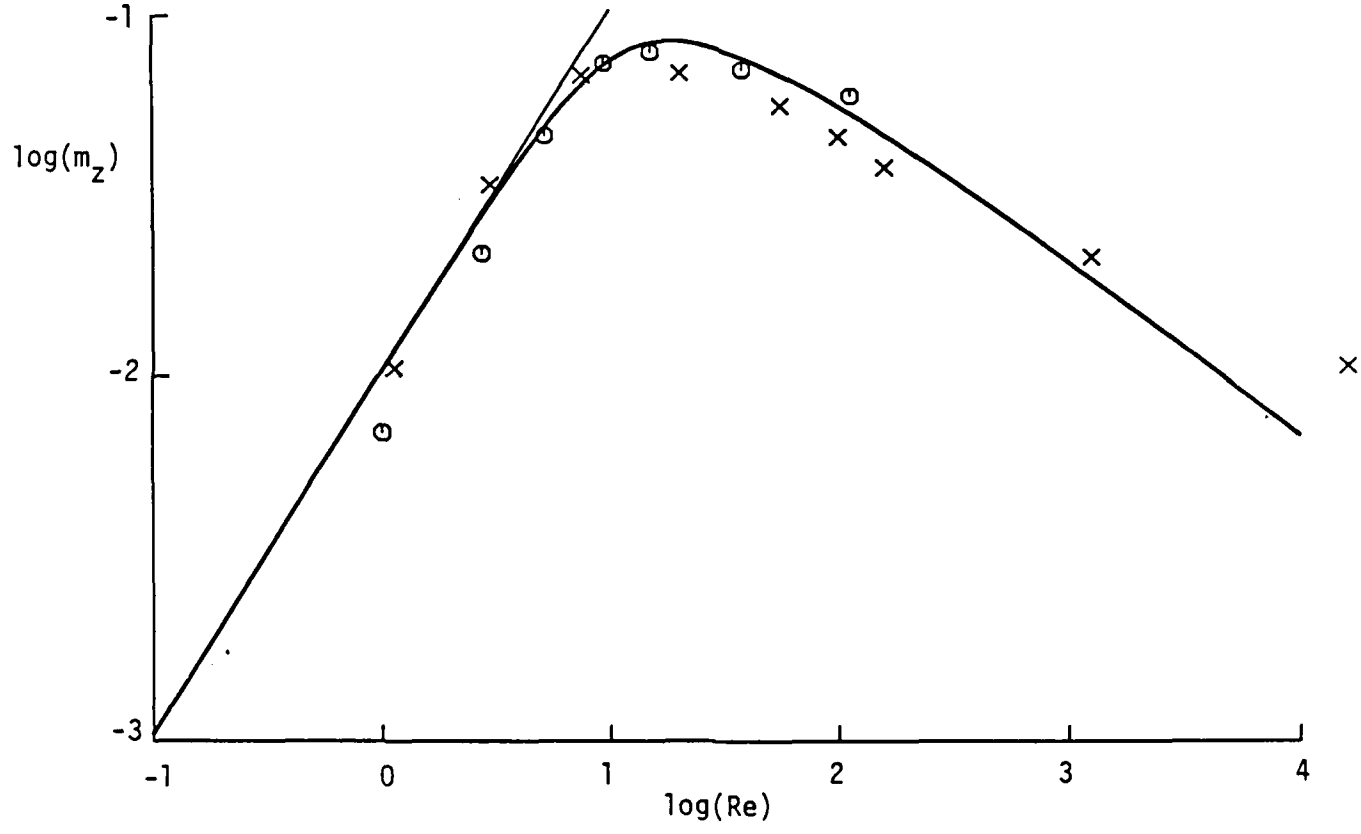

Figure 8.

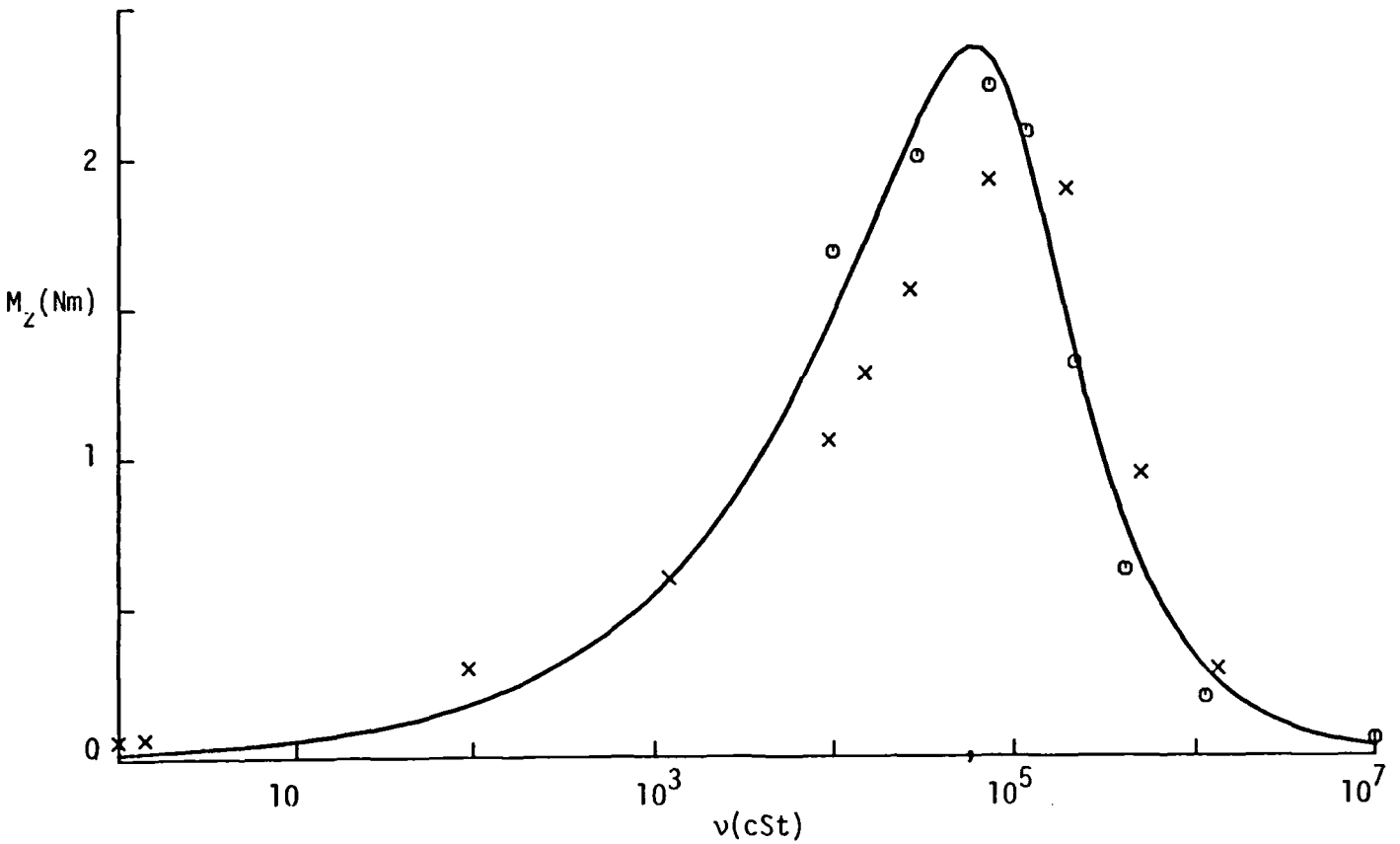

Figure 9.

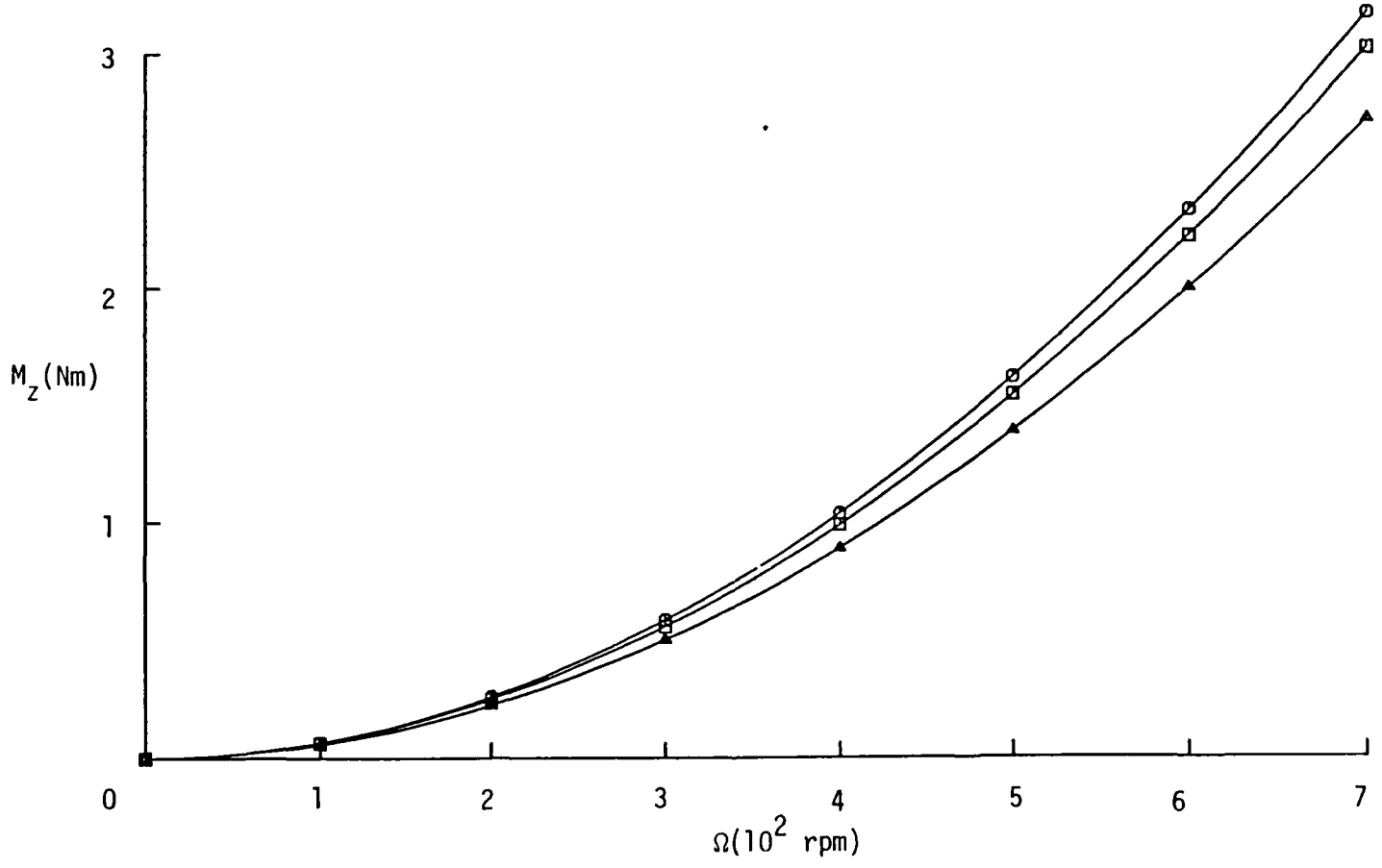

Figure 10.

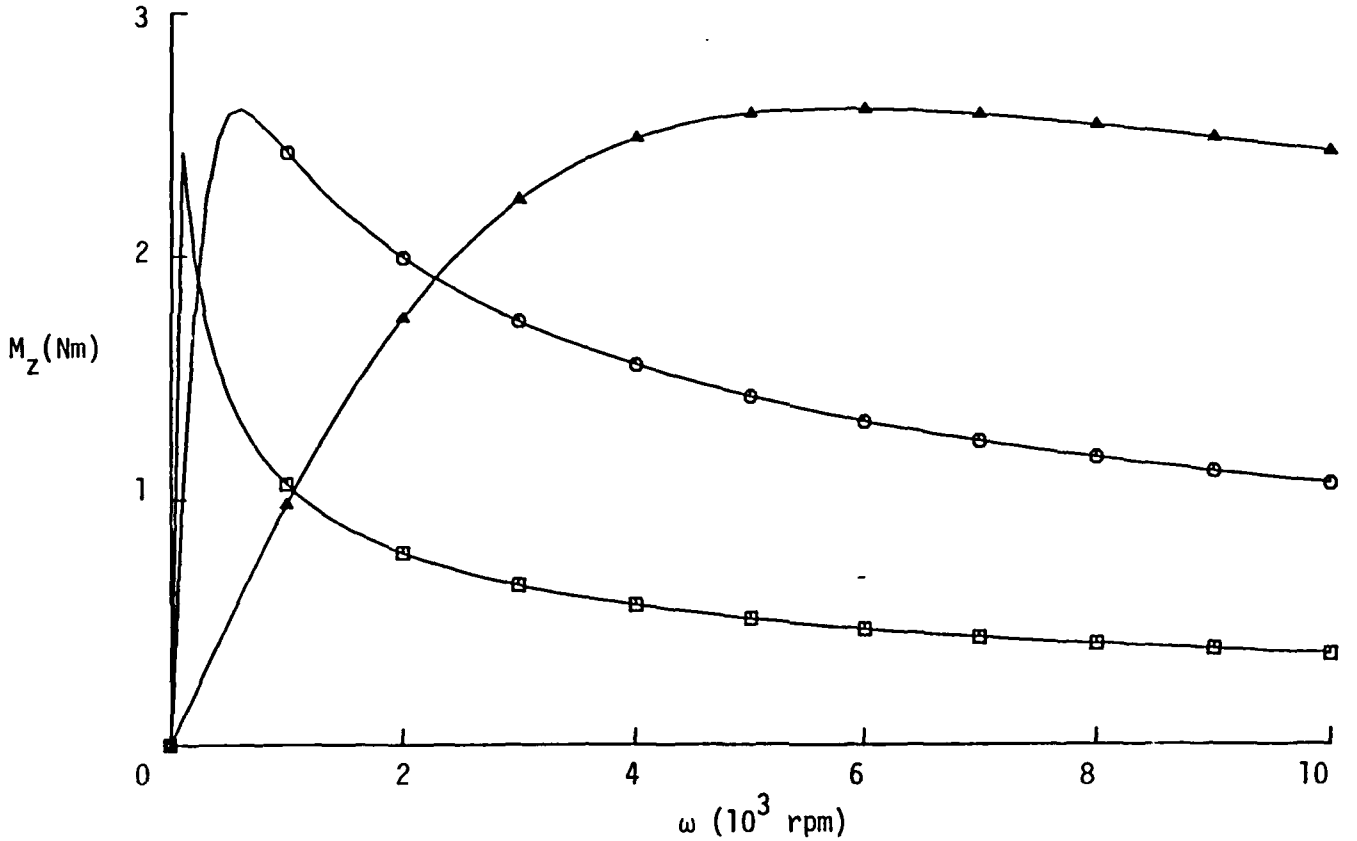

Figure 11.

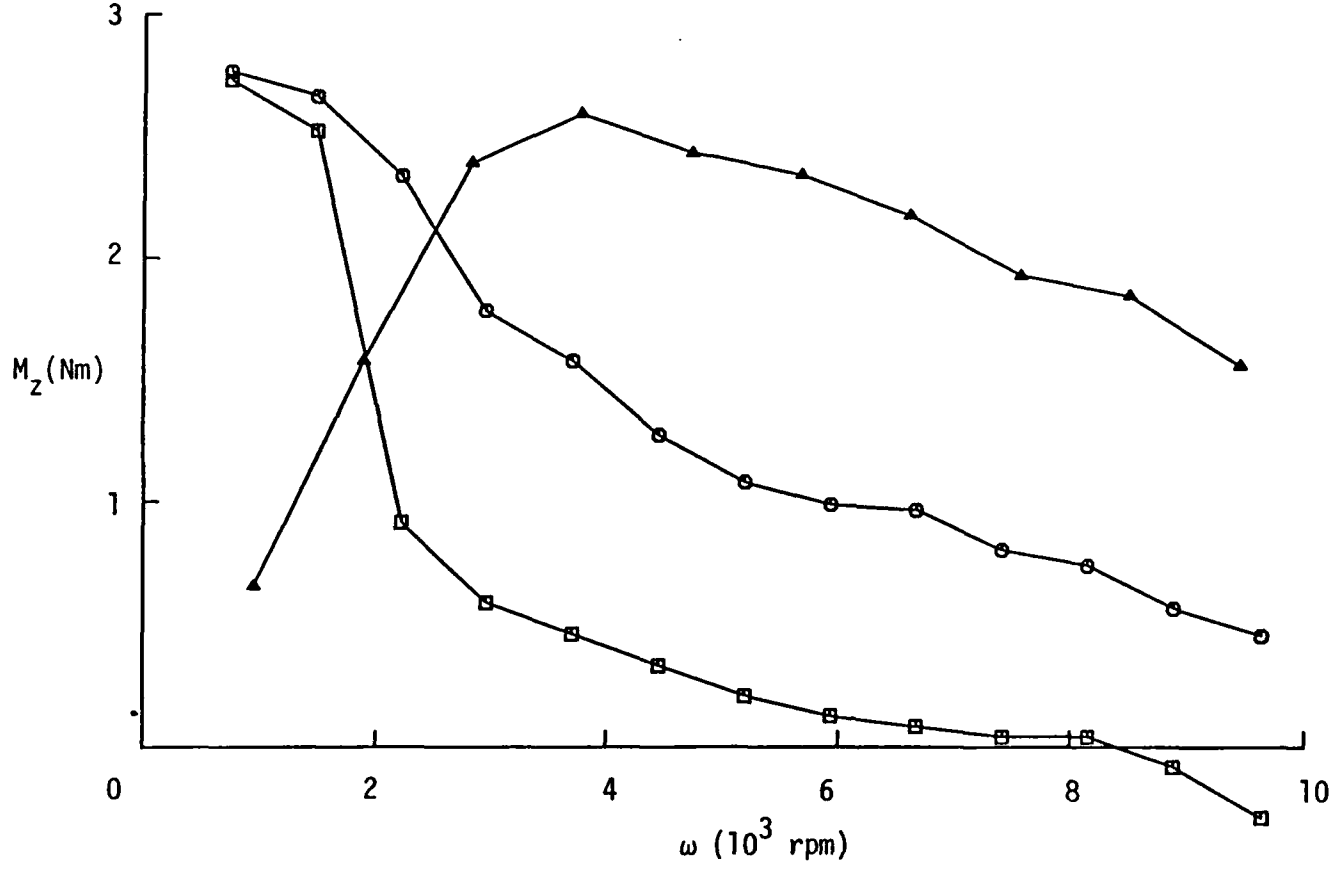

Figure 12.

Appendix B

Visualization of the Flow in a Spinning and Nutating Cylinder

by

Thorwald Herbert

David Pierpont

Department of Engineering Science and Mechanics
Virginia Polytechnic Institute and State University
Blacksburg, Virginia 24061

January 1986

Proceedings of the

1985 Scientific Conference on Chemical Defense Research

November 19-22, 1985
Aberdeen Proving Ground, Maryland

Visualization of the Flow in a Spinning and Nutating Cylinder

Thorwald Herbert

David Pierpont

Department of Engineering Science and Mechanics
Virginia Polytechnic Institute and State University
Blacksburg, Virginia 24061

Abstract

In the framework of a feasibility study, we have designed a small model test fixture for visualization of the flow in a spinning and nutating cylinder. We describe the apparatus and the visualization technique, and report some results. As the Reynolds number increases, we observe an axially almost uniform flow that turns at the ends, the development of two elongated cells in the plane of the spin and nutation axis, the formation of additional laminar cells, and ultimately unsteady and turbulent flow with a superposed large-scale cellular motion.

1. Introduction

It is well-known that spin-stabilized shells carrying liquid payloads can suffer dynamical instability. For cylindrical cavities and low viscosity of the liquid, the instability due to basically inviscid inertial waves is rather well understood[1]. The instability of certain shells like the XM761, however, is distinguished in character by the rapid loss in spin rate. Experiments[2] and subsequent field tests[3] establish that this flight instability is most pronounced for liquid fills of very high viscosity.

Theoretical analysis of a simple model of the internal flow[4] has provided some insight into the physical mechanisms of this instability, and rough information on flow velocity and despin moment. For sufficiently low Reynolds numbers, more detailed results for the velocity field have been obtained using computational methods for steady flows[5,6]. The flow phenomena at higher Reynolds numbers, however, are outside the scope of these methods, and it is not even clear whether the steady approach is justified.

Previous experiments at CRDC and BRL were carried out under full-scale conditions. These studies concentrated largely on global properties such as the moments exerted by the internal fluid motion. The yet most successful study of the field properties is Miller's observation of the void in a partially filled cylinder[7]. This study shows an axisymmetric void at low Reynolds numbers, a characteristic wavy distortion of the void at medium Reynolds numbers and an irregular (probably unsteady) liquid-air interface at high Reynolds number. Computational studies[5] indicate a cellular structure of the flow at a Reynolds number $Re = 45$, where $Re = \omega a^2/\nu$ is formed with the spin rate ω, the cylinder radius a and the kinematic viscosity ν. However, there is yet no link between numerical results and void observations. An attempt to trace buoyant beads with a movie camera[8] was very limited in revealing details of the velocity field. The limitations are due to distortion of the tracer path in the multi-media optical path involving curved surfaces, and to inevitable minute density differences in combination with high accelerations. Miller[8] used photochromic dye excited by a high-power pulsed laser in order to generate and record velocity profiles. Lighting problems in recording the pictures by a high-speed movie camera forced a reduction of the time scale, i.e. operation of the test fixture at lower spin rate, nutation rate, and kinematic

viscosity. Qualitative pictures of the small azimuthal velocity have been obtained. The efforts to provide more detailed data have been discontinued, however, due to continuing lighting problems, and the adverse off-design conditions at further reduced time scales.

In earlier work[9], we have proposed a drastic reduction of length and time scales for experimental studies, exploiting the principles of dynamical similarity. Following these considerations, we have designed and built a low-cost test fixture for flow visualization. In our qualitative approach, the length scale is reduced to 1/5, the time scale to 1/10, thus reducing moments by more than five orders of magnitude and velocities to 1/50. In spite of improvising and compromising in the interest of saving time and money, we have observed a wealth of phenomena from laminar, dominantly unidirectional flow through various stages of cellular motions to turbulent motions with a superposed cellular structure.

In the following we describe the principles underlying the design, the test fixture, the visualization technique, and some of our observations.

2. Dimensional Analysis

Evaluation of the experimental attempts to visualize the fluid flow clearly reveals the extreme full-scale conditions as evil. However, conclusive experiments can be conducted by exploiting the principles of dynamical similarity and appropriate scaling laws[9,4]. Between the three reference quantities, radius a, spin rate ω, and density ρ for length, time, and mass, respectively, the density of different fluids offers little variability. However, length scale and time scale can be easily changed. For dynamical similarity, the following dimensionless quantities must be kept fixed:

$\lambda = c/a$	aspect ratio
θ	nutation angle
$\tau = \Omega/\omega$	frequency
$Re = \rho\omega a^2/\mu$	Reynolds number

The nutation angle must remain the same in a scaled setup. Radius a and half-length c of the cylinder must be scaled by the same factor in order to keep the aspect ratio fixed. A second factor can be applied to both spin rate ω and nutation rate Ω, in order to preserve the frequency. Keeping Re fixed requires changing the kinematic viscosity $\nu = \mu/\rho$ by the same factor as ωa^2. Since the desired tendency is toward smaller radii and spin rates, we require less viscous fluids than those used in the full-scale experiments. Such fluids are easy to find.

It is obvious that the main thrust of an experiment may require specific optimum conditions. Flow visualization requires low velocities, i.e. low values of ωa. Measurements of moments require optimum values of $\omega^2 a^5$. Minimizing the rate of change of temperature requires a minimum of $\omega^3 a^2$. A good setup for flow visualization, therefore, may produce moments in a hardly measurable range.

3. The Test Fixture

The goal of our efforts was to show that a low-cost device ($\simeq$ \$500) can be designed for flow visualization. Details had to be kept simple. Accuracy and convenience had to compromise. Various preliminary concepts have been condensed into the design of a small apparatus that was built and explored as a senior student project[10]. The result of these efforts is shown in figure 1. A one-inch inner diameter cylinder of aspect ratio $\lambda = 4.3$ is used. The cylinder is cut from a pyrex glass tube with the inner diameter accurate within 1/5000 inch, but with varying wall thickness that affects the optical quality. The cylinder is filled with mixtures of water and glycerin. The mixing ratio is used to vary viscosity. On top, the cylinder is closed with a screwed-in plastic plug. A center hole allows access to the interior, especially for removing air bubbles. The hole can be closed using a toothpick.

The cylinder is glued to a drive plug and axis machined from a single piece of aluminum. The one-sided support allows easy (optical) access to the cylinder and permits using cylinders of different length. One-sided support is affordable due to the moments being approximately five orders of magnitude smaller than in the full-scale experiments. The axis is twice supported by ball bearings. The cylinder and shaft are driven via timing belts over exchangeable sets of pulleys by a $\leq$24V d.c. motor with sufficient torque in the range of 500 - 5000 rpm. Motor and cylinder support are mounted to an aluminum frame that can

be inclined to the vertical axis by approximately 5, 10, 15 and 20° using different support holes and struts.

The horizontal support plate is machined to leave the center position free for access and is screwed to a commercial record player (Garrard model 775). The plate can be offset in order to align the liquid's center of mass with the nutation axis. The record player provides nutation rates of 33, 45, and 78 rpm. The hollow axis is utilized to provide power to the spin motor. A nail with a smooth top and a brush fixed to the turntable proved sufficient for transmitting a single voltage to the motor. The remaining components of the experiment are: a Heathkit regulated power supply for the spin motor, a strobelight for controlled pulsed lighting, and suitable flow tracers. The strobelight (General Radio Strobotac) with adjustable frequency is used for lighting as well as for measuring the spin rate of the cylinder.

4. Visualization

As flow tracers we use Afflair 100 Silver Pearl, kindly donated by EM Chemicals, Hawthorne, NY. The material consists of very fine and shiny plastic platelets commercially used for cosmetic purposes. Although their specific weight is different from that of the fluid, the low accelerations in the scale model permit practically buoyant behavior of the platelets over considerable time.

At the slow time scale of the experiment, the fluid motion can be visually inspected while running the apparatus. At high viscosities, the apparatus can also be suddenly stopped, with the flow tracers "frozen" in the resting fluid. The platelets align with surfaces of constant shear. Therefore, by manually rotating the cylinder forth and back, the three-dimensional structure of the field can be inspected. This crude observation is very helpful in developing the visualization technique. A detailed account of the technique (appropriate particle density, pitfalls such as the history of particle distribution and alignment) has been given elsewhere[10].

Visualization of the frozen pattern can be essentially improved by using a light sheet passing through the spin axis. Sheet lighting enhances the clarity of the flow pattern by showing only the reflecting particles in a cut through the fluid. It reduces the undesirable reflections from the cylindrical surfaces and also enables photographic recording of the flow structure while the apparatus is in operation. A continuous light sheet is produced by a Spectra Physics model 120 (15 mW) helium-neon laser and a cylinder lens. In order to avoid the need for accurately firing the camera (35 mm Pentax with 50 mm lens) at a certain time, a cylindrical card board screen with a vertical slot and a 90° offset opening is fixed to the circumference of the turntable. The shutter is manually opened and closed after the laser sheet of light flashed 3 to 5 times through the slot.

5. Results

Some photographs taken with the apparatus in motion are shown in Figures 2-7. The figures show the flow pattern in the plane spanned by spin axis and nutation axis for $\theta = 21.3°$, $\Omega = 78$ rpm and different Reynolds numbers. Figure 2 shows that at Reynolds numbers as low as $Re = 20$ a cellular pattern develops with a pronounced symmetry about the axis as well as the midplane of the cylinder. At the present time it is unclear whether this pattern reflects the instantaneous velocity field. Symmetry arguments support viewing this pattern as originating from a nonlinear streaming term. As Re increases to $Re = 40$ (Figure 3), the pattern and its symmetry become more pronounced. At $Re = 50$ (Figure 4), additional cells develop near the cylinder's midplane. Simultaneously, the symmetry with respect to the cylinder axis is broken. A characteristic wavy distortion of the pattern near the axis develops that is more clearly shown in Figure 5 at $Re = 105$. While the cells disappeared, virtually axisymmetric bubbles occur at the end plates. At $Re = 140$ (Figure 6) these bubbles still persist. The bright, wavy line near the axis has broken into segments that are very much aligned like the void in Miller's observations. This pattern occurs only in the plane of spin axis and nutation axis and is therefore considered to represent the instantaneous velocity field. From the wealth of increasingly complex phenomena, Figure 7 finally shows a visualization at high $Re = 8000$. The random distribution of the particles in the interior most likely indicates turbulent flow. Nevertheless, the faint line near the axis resembles the characteristic centerline distortion of Figure 6, indicating a superposed large scale structure. The presence of such a large scale motion is also supported by the regular bands of particles deposited at the cylinder wall.

Specification of accurate Reynolds numbers suffers from some uncertainty in monitoring and measuring the wide range of viscosities for the hygroscopic water-glycerin mixtures exposed to uncontrolled thermal conditions. To within this uncertainty, however, the figures clearly reveal the cellular structure of the flow and the changes of the structure as the Reynolds number increases. Perhaps the most striking result of this visual study of the flow structure is the manifold of pattern at higher Reynolds numbers. A systematic analysis of these patterns has not been conducted. Although we found numerous opportunities for improvements, the feasibility of flow visualization with relatively simple means by proper scaling has been clearly demonstrated.

ACKNOWLEDGMENT

This experimental study is a digression from theoretical work supported by the Army Research Office under Contract DAAG29-82-K-0129 and by the Army AMCCOM under Contracts DAAK11-83-K-0011 and DAAA15-85-K-0012.

REFERENCES

1 Sedney, R. 1985 "A Survey of the Fluid Dynamic Aspects of Liquid-Filled Projectiles," AIAA Paper No. AIAA-85-1822-CP

2 Miller, M. C. 1982 "Flight Instabilities of Spinning Projectiles Having Nonrigid Payloads," *Journal of Guidance, Control, and Dynamics,* Vol. 5, pp. 151-157.

3 D'Amico, W. P. & Miller, M. C. 1979 "Flight Instability Produced by a Rapidly Spinning, Highly Viscous Liquid," *Journal of Spacecraft and Rockets,* Vol. 16, pp. 62-64.

4 Herbert, Th. 1985 "Viscous Fluid Motion in a Spinning and Nutating Cylinder", to appear in Journal of Fluid Mechanics.

5 Vaughn, H. R., Oberkampf, W. L. & Wolfe, W. P. 1985 "Fluid Motion Inside a Spinning Nutating Cylinder," Journal of Fluid Mechanics, Vol. 150, pp. 121-138.

6 Nagel, Y. & Strikwerda, J. 1985 "A Numerical Study of Flow in Spinning and Coning Cylinders," in these Proceedings.

7 Miller, M. C. 1981 "Void Characteristics of a Liquid Filled Cylinder Undergoing Spinning and Coning Motion," J. of Spacecraft and Rockets, Vol. 18, pp. 286-288.

8 Miller, M. C. 1984 "Visualization Studies of Viscous Liquid Flow in a Spinning and Coning Cylinder," Proc. 1984 Scientific Conference on Chemical Defense Research, (Ed. M. Rausa), Report CRDC-SP-85006, pp. 541-546.

9 Herbert, Th. 1982 "Fluid Motion in a Rotating and Nutating Cylinder - Part I," Report prepared under the Scientific Services Program. Published as Report CRDC-CR-84087, 1984

10 Pierpont, D. 1985 "Design of an Experiment for Visualization of the Flow in a Spinning and Nutating Cylinder," Senior Project Report, VPI & SU.

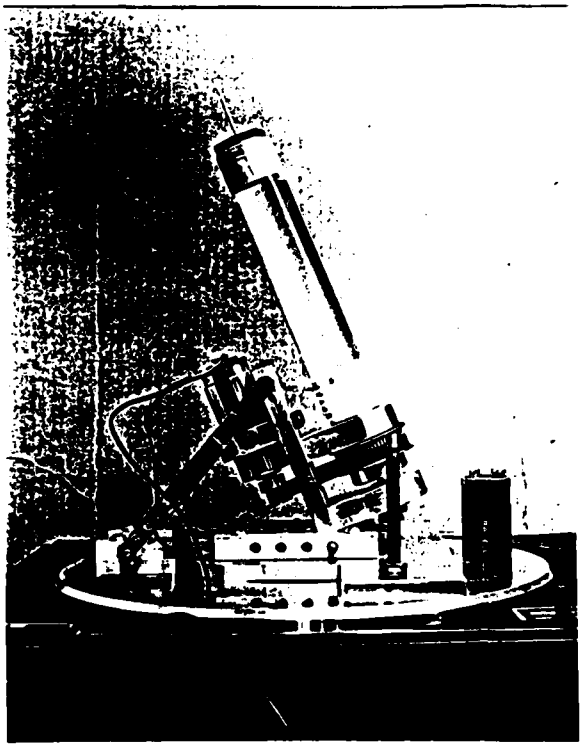

Figure 1

The miniature test fixture. The inner radius of the cylinder is $a = 1.27$ cm, the aspect ratio 4.3.

Figure 2

$\theta = 21.3°$
$\Omega = 78$ rpm
$\nu = 240$ cSt
$\omega = 300$ rpm
$Re = 20$

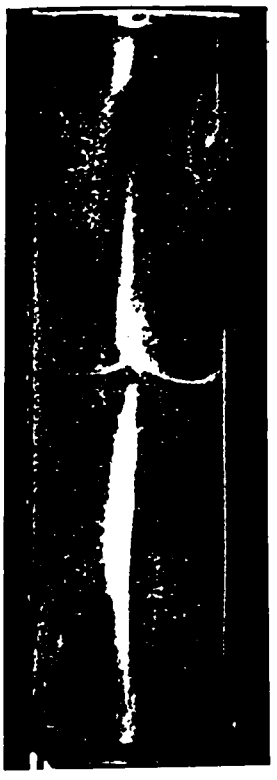

Figure 3

$\theta = 21.3°$
$\Omega = 78$ rpm
$\nu = 240$ cSt
$\omega = 600$ rpm
$Re = 40$

Figure 4

θ =21.3°
Ω = 78 rpm
ν =240 cSt
ω = 750 rpm
Re = 50

Figure 5

θ =21.3°
Ω = 78 rpm
ν = 70 cSt
ω = 450 rpm
Re = 105

Figure 6

θ =21.3°
Ω = 78 rpm
ν =70 cSt
ω = 600 rpm
Re = 140

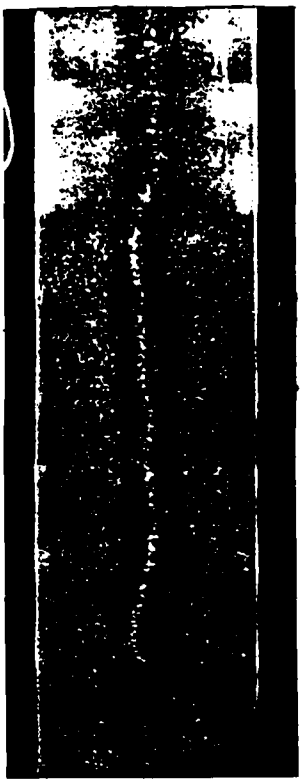

Figure 7

θ =21.3°
Ω = 78 rpm
ν = 0.95 cSt
ω = 450 rpm
Re = 8000

END

DTIC

7-86